Annual Review of Earth and Planetary Sciences

Subduction-Driven Volatile Recycling: A Global Mass Balance

D.V. Bekaert,[1,*] S.J. Turner,[2] M.W. Broadley,[3] J.D. Barnes,[4] S.A. Halldórsson,[5] J. Labidi,[6] J. Wade,[7] K.J. Walowski,[8] and P.H. Barry[1,*]

[1]Marine Chemistry and Geochemistry Department, Woods Hole Oceanographic Institution, Woods Hole, Massachusetts 02543, USA; email: pbarry@whoi.edu

[2]Department of Geosciences, University of Massachusetts, Amherst, Massachusetts 01003, USA

[3]Centre de Recherches Pétrographiques et Géochimiques, CNRS UMR 7358, Université de Lorraine, F-54501 Vandoeuvre-lès-Nancy, France

[4]Department of Geological Sciences, Jackson School of Geosciences, The University of Texas at Austin, Austin, Texas 78712, USA

[5]Nordic Volcanological Center, Institute of Earth Sciences, University of Iceland, Reykjavik, Iceland 600169-2039

[6]Université de Paris, Institut de physique du globe de Paris, CNRS, F-75005 Paris, France

[7]Department of Earth Sciences, University of Oxford, Oxford OX1 3AN, United Kingdom

[8]Department of Geology, Middlebury College, Middlebury, Vermont 05753, USA

Annu. Rev. Earth Planet. Sci. 2021. 49:37–70

First published as a Review in Advance on October 16, 2020

The *Annual Review of Earth and Planetary Sciences* is online at earth.annualreviews.org

https://doi.org/10.1146/annurev-earth-071620-055024

*Joint first author

Keywords

volatiles, subduction, recycling, mass balance, volcano, mantle

Abstract

Volatile elements (water, carbon, nitrogen, sulfur, halogens, and noble gases) played an essential role in the secular evolution of the solid Earth and emergence of life. Here we provide an overview of Earth's volatile inventories and describe the mechanisms by which volatiles are conveyed between Earth's surface and mantle reservoirs, via subduction and volcanism. Using literature data, we compute volatile concentration and flux estimates for Earth's major volatile reservoirs and provide an internally balanced assessment of modern global volatile recycling. Using a nitrogen isotope box model, we show that recycling of N (and possibly C and S) likely began before 2 Ga and that ingassing fluxes have remained roughly constant since this time. In contrast, our model indicates recycling of H_2O

(and most likely noble gases) was less efficient in the past. This suggests a decoupling of major volatile species during subduction through time, which we attribute to the evolving thermal regime of subduction zones and the different stabilities of the carrier phases hosting each volatile.

- This review provides an overview of Earth's volatile inventory and the mechanisms by which volatiles are transferred between Earth reservoirs via subduction.
- The review frames the current thinking regarding how Earth acquired its original volatile inventory and subsequently evolved through subduction processes and volcanism.

1. INTRODUCTION

1.1. Volatile Elements and Their Importance for the Earth System

Goldschmidt (1954) originally classified the atmophile elements (N, C, H, and noble gases) as those marked by extreme volatility, concentrated in the atmosphere and hydrosphere. Due to the prevalence of volatile and biologically relevant elements at Earth's surface, our planet has maintained a habitable climate (Bergin et al. 2015) since at least 3.4 Ga (Javaux 2019). However, significant quantities of volatiles also reside in the solid Earth, stored since accretion (e.g., Williams & Mukhopadhyay 2019, Labidi et al. 2020) or introduced over geological history by subduction (e.g., Holland & Ballentine 2006). Volatile elements mediate the rheological properties of the mantle and thus critically affect mantle convection, melt generation, plate tectonics, and continental crust formation (e.g., McGovern & Schubert 1989). Major volatiles, such as H_2O and CO_2, act to depress the melting point of mantle lithologies, which dictates the physical and chemical characteristics of erupted lavas (Holloway & Jakobsson 1986). Despite the terrestrial mantle's relatively low volatile element abundances, it represents 99.4 wt% of the bulk silicate Earth by mass (Schaefer et al. 2012) and can therefore exert a significant influence on the volatile inventory of Earth's surface.

Volatile: element with a low boiling point that is significantly outgassed from subaerial volcanoes and usually concentrated at planetary surfaces

Subduction: downward movement of an oceanic plate into the mantle beneath a less dense plate (typically continental)

Mantle convection: slow creeping motion of Earth's solid silicate mantle caused by convection currents in which hot material rises and cold material sinks

Chondrites: most pristine meteorites that formed through dust coagulation in the protosolar nebula and have not been subsequently modified

Protosolar nebula: rotationally flattened cloud of gas and dust from which the Sun and planets formed

1.2. The Origin of Volatiles on Earth

Earth likely formed via heterogeneous accretion of solid materials originating from various heliocentric distances in the early Solar System (Rubie et al. 2015). Depending on their origin, the rocky building blocks of Earth comprised variable amounts of volatile elements that were subsequently redistributed during planetary differentiation and geological processes to shape Earth's surface into a hospitable environment for life. There are two main sources of volatile elements commonly considered in planetary formation. The first source is composed of chondritic material, which corresponds to the building blocks of Earth's main accretion event (e.g., Holland et al. 2009, Broadley et al. 2020) as well as late accretion (Marty 2012). Although chondritic materials that formed Earth would predominantly originate from the dry inner regions of the Solar System (e.g., Dauphas 2017), pristine carbonaceous chondrites from the outer Solar System are rich in major volatiles (up to ~10 wt% H_2O, several wt% C, and ~0.1 wt% N) and, if included in Earth's accretionary material, could have largely contributed to the terrestrial volatile budget (Marty 2012). The second potential source of planetary volatiles is protosolar nebula gas, which surrounded planetary embryos at the time of their formation. Planets that formed before the dissipation of the protosolar nebula [i.e., within ~4 Myr after the start of the Solar System (Wang et al. 2017)] may have gravitationally captured part of the protosolar nebula gas, which could be retained in the present-day Earth and constitute a significant source of terrestrial volatile

elements (Wu et al. 2018). Evidence for protosolar nebula–derived volatiles within terrestrial planets comes from H isotopes (Hallis et al. 2015) and Ne isotopes within deep mantle–derived samples (Yokochi & Marty 2004, Williams & Mukhopadhyay 2019), suggesting that proto-Earth acquired and retained at least part of its volatile inventory very early in the history of the Solar System. Part of these accretionary volatiles was subsequently transferred to the Earth's surface over geological times via heterogeneous degassing of the solid Earth to form the atmosphere (Bekaert et al. 2019).

1.3. Recycling and Redistribution of Volatiles Throughout the Earth System

Volatile recycling between present-day Earth reservoirs is driven by plate tectonics, active slab subduction, mantle convection, and volcanism, which distribute volatiles and enable exchange of material between Earth's surface and interior (**Figure 1**). Subduction zones represent a key interface where vertical mass transfer of volatiles occurs, whereby material is transported past mantle depths relevant for arc magma genesis (Wilson et al. 2014). Although the timing of the onset of plate tectonics is debated, geochemical data suggest that subduction has been active since at least the Paleoarchean (Richardson et al. 2001, Shirey & Richardson 2011) and as early as the Hadean (Hopkins et al. 2008, Korenaga 2013, Keller & Schoene 2018). Subduction would initially have occurred at relatively high temperatures (i.e., hot subduction), implying limited transfer of volatiles into the solid Earth (Brown 2006, van Hunen & Moyen 2012, Duncan & Dasgupta 2017). The onset of modern-style subduction (i.e., cold subduction) marked a fundamental change in the nature of Earth's mantle-surface interaction (Holder et al. 2019) with surface volatiles being efficiently transported back into the solid Earth. Constraining the timing of the onset of cold subduction and evolution of volatile recycling efficiency over geological time is critical for understanding the present-day volatile inventories of Earth's mantle and surface reservoirs.

Heavy noble gas (HNG) (Ar, Kr, Xe) data indicate that a large fraction of volatile elements presently in Earth's mantle were recycled via subduction of surface components over the past ~2–3 Gyr (e.g., Holland & Ballentine 2006, Parai & Mukhopadhyay 2015). However, the efficiency of this recycling process depends on the respective ingassing/outgassing efficiencies of each volatile, with light noble gases (He, Ne), for example, being marginally recycled, if at all. The pervasiveness of modern-like atmospheric Xe in the mantle suggests that significant volatile recycling into the convecting mantle did not occur prior to 2.5 Ga (Parai & Mukhopadhyay 2018). Further evidence for volatile recycling is provided by mass-dependent fractionation S isotope signatures from various hotspots (Labidi et al. 2013, 2015; Dottin et al. 2020a). Rare mass-independent isotopic S isotope signatures in the source of some hotspots indicate significant S recycling occurred prior to 2.5 Ga and requires the contribution of Archean supracrustal components (Cabral et al. 2013, Dottin et al. 2020b). This apparent contrast between Xe and S isotope constraints on the timing of the onset of volatile recycling illustrates either (*a*) decoupling between major volatile species during subduction or (*b*) that distinct mantle reservoirs experienced contrasted histories of volatile recycling. Additional suggestions of volatile recycling are numerous, including evidence for the presence of recycled C in certain enriched mid-ocean ridge basalt (MORB) samples (with $C/^3He$ that correlate with K/Ti) (Marty & Zimmermann 1999), water and D/H systematics of modern hotspots (Shaw et al. 2012, Loewen et al. 2019) and komatiites (Sobolev et al. 2019), high $N/^3He$ and $C/^3He$ ratios in ^{4}He-rich hotspots (Marty & Dauphas 2003), and the analysis of silicate mineral inclusions in diamonds (Walter et al. 2008). These geochemical constraints are consistent with those derived from petrological analysis of exhumed metamorphic rocks, indicating that Earth's modern plate tectonic regime, characterized by cold subduction, has developed gradually with the secular cooling of the mantle since the Neoarchean era (Brown 2006, Holder et al. 2019).

Slab: the portion of a tectonic plate that is being subducted

Hot subduction: when the downgoing slab is marked by relatively hot geotherms, causing extensive loss and fractionation of its volatile inventory

Cold subduction: when the downgoing slab is marked by relatively cold geotherms and is therefore able to retain volatiles with minimal fractionation

Volatile recycling efficiency: fraction (%) of the slab inventory that is transported to the mantle (i.e., net ingassing flux/initial slab inventory)

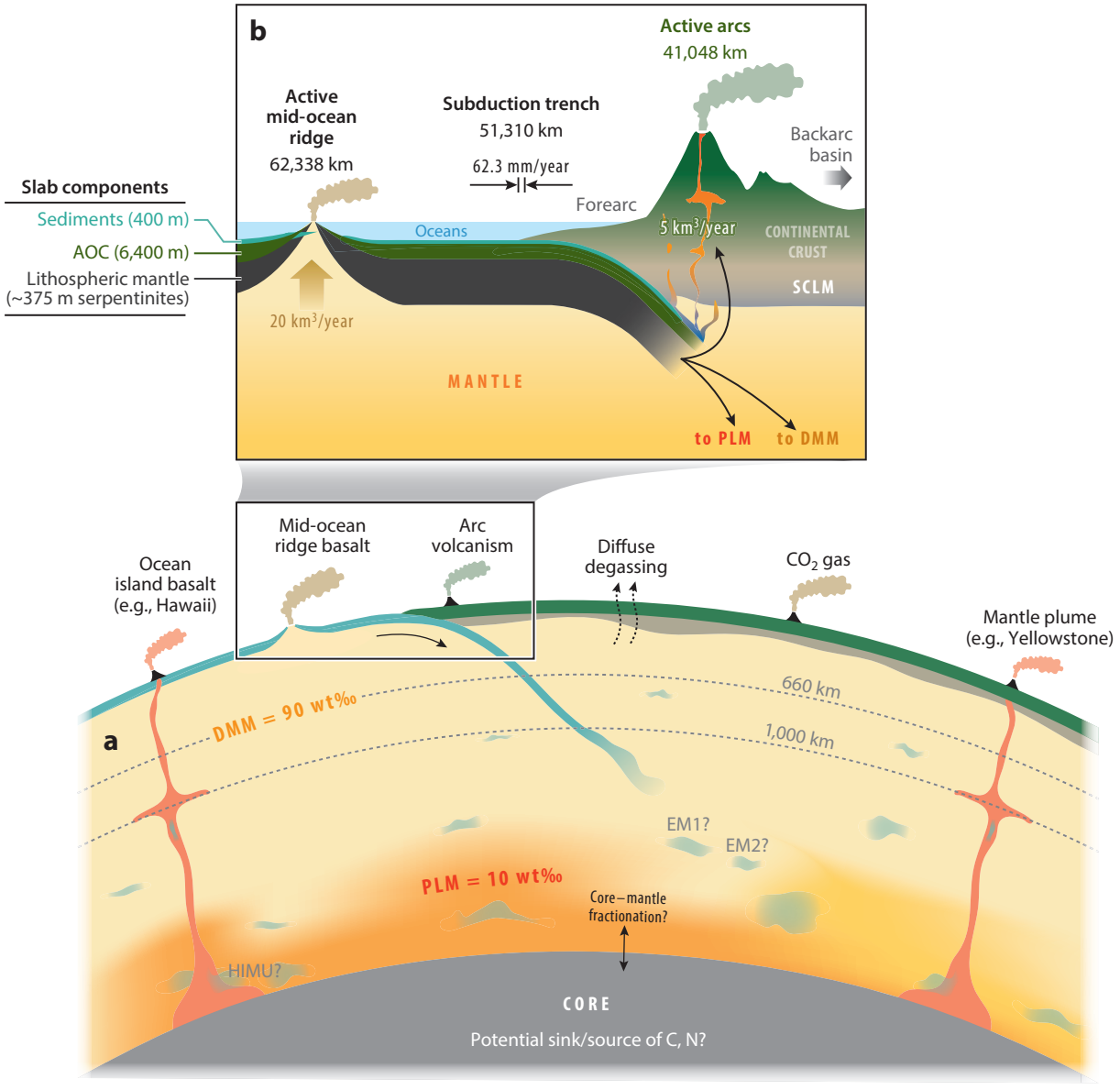

Figure 1

Diagram showing (*a*) mantle volatile reservoirs (PLM, DMM) and (*b*) the movement of volatiles through the subduction zone. Mantle volatiles are primarily transferred to crustal and atmospheric reservoirs by partial mantle melts at volcanic arcs, mid-ocean ridges, and plume-derived volcanic systems. At the surface, mantle-derived volatiles are released in volcanically active regions via volcanic eruptions, springs, fumarolic activity, and diffuse degassing. Assumptions regarding the slab thickness, magma production rates, trench and ridge lengths, and convergence rate (which constitute the parameters of our internally consistent mass-balance model) are shown in panel *b* (Bird 2003) (see Section 2.1). Abbreviations: AOC, altered oceanic crust; DMM, depleted mid-ocean ridge basalt mantle; EM1/EM2, enriched mantle 1/enriched mantle 2; HIMU, high μ mantle domain; PLM, primitive lower mantle or plume mantle; SCLM, subcontinental lithospheric mantle.

Despite the importance of recycling processes for mantle and surface volatile inventories, quantifying which volatile elements have been recycled within the solid Earth remains a subject of considerable debate. For example, there is substantial uncertainty about (*a*) how recycling of surficial material has affected the isotopic composition of volatile elements and their budgets in shallow versus deep mantle reservoirs (e.g., Jambon 1994), (*b*) how the flux balance between volatile outgassing (through volcanism) and ingassing (through subduction) has changed since the onset of volatile recycling (Hilton et al. 2002), and (*c*) how this outgassing/ingassing balance controlled the evolution of the surface inventory through time.

Subcontinental lithospheric mantle (SCLM): cold, old, uppermost solid part of Earth's mantle associated with the continental lithosphere that is not actively convecting

Mid-ocean ridge (MOR): submarine volcanic chain where seafloor spreading occurs along a divergent plate boundary; MORBs are basalts erupted at MORs

Supplemental Material >

1.4. Review Aims and Approach

Here we provide a comprehensive overview of volatile concentrations in slab and mantle reservoirs (**Table 1**), as well as global volatile inventories and fluxes (**Table 2**) associated with subduction (influxes) (Section 3) and volcanic outgassing (outfluxes) (Section 4). Flux values have been made internally consistent by balancing magmatic production and plate subduction rates. Taken together, these data are used to derive a new global mass balance of terrestrial volatiles (Section 5.1). We use a box model for N that predicts subduction began ca. 2 Ga and that ingassing fluxes remained roughly constant until present. We then explore the implications of this model for the evolution of Earth's surface volatile inventory and behavior of volatile elements during subduction. We provide a user-friendly **Supplemental Spreadsheet** as well as **Supplemental MATLAB** code for calculations (see the **Supplemental Materials** and **https://zenodo.org/record/4141172#.X5huTh1Cdds**).

2. SURFACE VOLATILE RESERVOIRS

The volatile compositions of Earth's atmosphere and oceans have been well constrained and represent the reference point for our understanding of Earth's volatile budget. Estimates of volatile concentrations in the surface reservoir (i.e., atmosphere + oceans + sediments + continental and oceanic crusts) are from previous literature compilations (see **Table 2** and references therein). The volatile inventory of the continental crust is likely significant but poorly constrained, and here we assume its contribution to the global volatile mass balance to be relatively small. Notably, the continental crust and subcontinental lithospheric mantle (SCLM) are isolated from the convecting mantle over billions of years, implying that, unlike other reservoirs, they are not an integral part of the global cycle of volatile elements between the mantle and Earth's surface (**Supplemental Text Section 6.1**; Section 6.1). We emphasize that, in the framework of our global mass balance, any volatile that is degassed to the atmosphere/oceans via volcanism, or emitted at mid-ocean ridges (MORs) and incorporated into the oceanic crust, is considered to be included in the surface reservoir. Volcanism and subduction therefore represent the dominant mechanisms through which volatiles are respectively added to, and removed from, the surface inventory. Inputs of volatiles to the surface reservoir can be estimated from volatile flux measurements at volcanoes, but assessing the global efficiency of surface volatile removal via subduction requires typical slab volatile composition to be defined.

2.1. Defining a Typical Slab Composition

Downgoing slabs consist of marine sediments, altered oceanic crust (AOC), and partially serpentinized lithospheric mantle (e.g., Hacker 2008). We emphasize that the relative thickness, composition, and ultimate contribution of these three components to slab volatile inventories may vary

Table 1 Best estimates of volatile concentrations in slab components (AOC, serpentinites, sediments), bulk slab, and DMM and PLM sources

Concentration (mol/g)	AOC (d: 3.00 g/cm^3)[a]	Serpentinites (d: 2.6 g/cm^3)[b]	Sediments (d: 1.7 g/cm^3)[c]	Typical slab (best estimate)[d]	DMM source[e,f]	PLM source[e,g]
^{14}N	7.00×10^{-07} (0.93:13.0)	1.71×10^{-07} (0.93:3.21)	3.03×10^{-05} (0.71:14.3)	1.64×10^{-06}	$(2.88^{+2.02}_{-1.35}) \times 10^{-08}$	$(1.93^{+0.99}_{-1.01}) \times 10^{-07}$
^{3}He	N/S	N/S	N/S	N/S	$(1.36^{+0.19}_{-0.19}) \times 10^{-15}$	$(2.33^{+0.96}_{-0.96}) \times 10^{-14}$
^{22}Ne	1.55×10^{-15} (0.77:4.64)	8.51×10^{-14} (0.07:36.8)	4.06×10^{-15} (0.64:8.19)	5.54×10^{-15}	$(2.77^{+0.39}_{-0.39}) \times 10^{-16}$	$(7.84^{+3.78}_{-3.45}) \times 10^{-15}$
^{36}Ar	8.92×10^{-14} (4.46:26.8)	3.03×10^{-12} (0.18:19.0)	4.30×10^{-12} (0.84:11.6)	3.64×10^{-13}	$(3.40^{+0.48}_{-0.48}) \times 10^{-15}$	$(2.84^{+1.85}_{-1.45}) \times 10^{-14}$
^{84}Kr	3.21×10^{-15} (1.61:9.64)	1.07×10^{-13} (0.03:7.02)	6.01×10^{-13} (0.38:17.0)	2.76×10^{-14}	$(9.64^{+1.36}_{-1.36}) \times 10^{-17}$	$(2.59^{+1.65}_{-1.31}) \times 10^{-15}$
^{130}Xe	1.78×10^{-16} (1.34:7.14)	2.04×10^{-15} (0.04:14.9)	1.00×10^{-14} (0.07:2.63)	5.85×10^{-16}	$(1.79^{+0.25}_{-0.25}) \times 10^{-18}$	$(3.69^{+3.01}_{-2.14}) \times 10^{-17}$
H_2O	5.55×10^{-04} (2.22:9.99)	7.22×10^{-03} (6.66:7.22)	3.94×10^{-03} (2.78:8.33)	9.77×10^{-04}	$(1.32^{+0.38}_{-0.38}) \times 10^{-05}$	$(3.89^{+1.22}_{-1.67}) \times 10^{-05}$
^{12}C	4.16×10^{-05} (3.33:5.00)	4.25×10^{-05} (1.25:7.24)	2.16×10^{-03} (0.25:6.66)	1.11×10^{-04}	$(2.99^{+1.35}_{-1.12}) \times 10^{-06}$	$(9.77^{+1.14}_{-1.14}) \times 10^{-06}$
S	3.43×10^{-05} (0.28:4.02)	2.85×10^{-05} (0.56:5.14)	1.64×10^{-04} (0.16:3.12)	3.83×10^{-05}	$(6.08^{+0.73}_{-0.63}) \times 10^{-06}$	$(8.89^{+1.72}_{-0.93}) \times 10^{-06}$
Cl	5.58×10^{-06} (2.84:11.9)	1.78×10^{-05} (1.13:3.81)	1.33×10^{-05} (0.61:2.15)	6.40×10^{-06}	$(1.69^{+0.33}_{-0.33}) \times 10^{-07}$	$(8.12^{+1.58}_{-1.50}) \times 10^{-07}$
F	5.68×10^{-06} (1.96:11.3)	1.95×10^{-06} (0.79:3.42)	3.07×10^{-05} (2.66:3.94)	6.32×10^{-06}	$(6.25^{+1.14}_{-1.14}) \times 10^{-07}$	$(1.14^{+0.12}_{-0.12}) \times 10^{-06}$
Br	7.73×10^{-09} (1.56:18.6)	6.88×10^{-08} (5.63:9.01)	4.00×10^{-07} (2.68:5.26)	2.34×10^{-08}	$(2.10^{+0.61}_{-0.61}) \times 10^{-10}$	$(1.01^{+0.29}_{-0.29}) \times 10^{-09}$
I	7.09×10^{-11} (2.47:29.9)	4.57×10^{-09} (0.58:54.4)	1.18×10^{-07} (0.56:1.98)	4.13×10^{-09}	$(2.84^{+1.52}_{-1.52}) \times 10^{-12}$	$(1.36^{+0.73}_{-0.73}) \times 10^{-11}$

Uncertainties reflect the ranges of values in the literature, except for halogens, whose concentrations have been compiled from multiple studies; we report the median values and interquartile ranges (details in the **Supplemental Spreadsheet**). Abbreviations: AOC, altered oceanic crust, DMM, depleted mid-ocean ridge basalt mantle; MORB, mid-ocean ridge basalt; N/S, not subducted; PLM, primitive lower mantle or plume mantle.

[a]AOC: N: Li et al. (2007), Busigny et al. (2019); noble gases: Chavrit et al. (2016), using AOC concentrations for ^{36}Ar and ^{130}Xe and the ^{22}Ne/^{36}Ar and ^{84}Kr/^{36}Ar ratios of seawater (Kendrick et al. 2013) to derive ^{22}Ne and ^{84}Kr contents; H_2O: Carlson & Miller (2003), Jarrard (2003); C: Plank & Manning (2019); S: Alt (1995), Alt & Shanks (2011); halogens: Barnes & Cisneros (2012), Chavrit et al. (2016), Zhang et al. (2017), Kendrick (2019a,b).

[b]Serpentinites: N: Halama et al. (2014); noble gases: Kendrick et al. (2013); H_2O: Ulmer & Trommsdorff (1995); C: Alt et al. (2012); S: Alt et al. (2012); halogens: Barnes & Sharp (2006), John et al. (2011), Kendrick et al. (2011, 2013), Kobayashi et al. (2017).

[c]Sediments: N: Li & Bebout (2005), Busigny et al. (2011); noble gases: Matsuda & Nagao (1986), Staudacher & Allègre (1988); H_2O: Plank (2014); C: Plank & Manning (2019); S: Berner & Raiswell (1984), Plank (2014); halogens: Muramatsu & Wedepohl (1998), Barnes et al. (2008, 2009), John et al. (2011), Kendrick et al. (2018), Muramatsu et al. (2007).

[d]The bulk slab composition is calculated from assumptions reported in **Figure 1**.

[e]For both DMM and PLM, volatile concentrations and outfluxes are related by a unique degree of partial melting (11% and 9% for the DMM and PLM, respectively) and magma production rate (20 km^3/year and 1.21 km^3/year, respectively). The partition coefficient of H_2O is considered identical to that of Ce [0.022 (Workman & Hart 2005)].

[f]DMM source: noble gas concentrations computed from the ^{3}He flux by Holzer et al. (2017) and noble gas elemental ratios of popping rocks (Moreira et al. 1998); N: computed from ^{36}Ar using the N/^{36}Ar from Marty & Dauphas (2003); H_2O: Le Voyer et al. (2017); C: two methods: first, from the ^{3}He flux by Holzer et al. (2017) and C/^{3}He by Javoy & Pineau (1991), Marty & Zimmermann (1999), Resing et al. (2004); and second, from Le Voyer et al. (2019); S: Nielsen et al. (2014); halogens: two methods (**Supplemental Table 2**): first, from compilation of literature estimates (**Supplemental Table 2**; **Supplemental Spreadsheet**); and second, by coupling the F/Pr and Cl/K measured in MORB glasses (Kendrick et al. 2017) with mantle concentration of Pr (Workman & Hart 2005) and K (Arevalo et al. 2009), and then using the DMM Cl concentration together with the Br/Cl and I/Cl of MORB glasses (Kendrick et al. 2017) to derive Br and I contents.

[g]PLM source: N: Marty & Dauphas (2003); noble gas: ^{3}He from Gonnermann & Mukhopadhyay (2007, 2009), elemental ratios from Mukhopadhyay (2012) (for Ne, Ar, and Xe) and Trieloff et al. (2002) (for Kr); H_2O: Simons et al. (2002); C: Tucker et al. (2019); S: Labidi et al. (2015), Lorand & Luguet (2016); halogens: F and Cl concentrations from the measured Pr (Jackson & Jellinek 2013) and modeled K (Arevalo et al. 2009) concentrations of the PLM. The Br/Cl and I/Cl from Kendrick et al. (2015, 2017) are then used to derive the Br and I contents of the PLM.

Supplemental Material >

Table 2 Best estimates of volatile inventories in surface, DMM, and PLM reservoirs, as well as total fluxes into and out of the mantle

	Inventories (mol)			Flux in (mol/year) (best estimates)			Fluxes out (mol/year)[e]		
	Surface[a]	DMM source (90 wt% of bulk mantle)[b]	PLM source (10 wt% of bulk mantle)[b]	In from slab (no serpentinite)[c]	In from slab (total)[c]	Recycling efficiencies (%)[d]	Out from arcs[f]	Out from DMM[g]	Out from PLM[g]
^{14}N	3.57×10^{20}	$(1.04^{+0.73}_{-0.49}) \times 10^{20}$	$(7.74^{+3.98}_{-4.03}) \times 10^{19}$	1.09×10^{11}	1.09×10^{11}	38 (36:38)	$(6.72^{+0.22}_{-0.22}) \times 10^{10}$	$(1.58^{+1.11}_{-0.74}) \times 10^{10}$	$(7.76^{+3.99}_{-4.04}) \times 10^{09}$
^{3}He	9.14×10^{13}	$(4.91^{+0.69}_{-0.69}) \times 10^{12}$	$(9.34^{+3.83}_{-3.83}) \times 10^{12}$	N/S	N/S	N/S	$(7.39^{+2.30}_{-2.30}) \times 10^{01}$	$(7.45^{+1.05}_{-1.05}) \times 10^{02}$	$(9.35^{+3.84}_{-3.84}) \times 10^{02}$
^{22}Ne	1.36×10^{14}	$(1.00^{+0.14}_{-0.14}) \times 10^{12}$	$(3.14^{+1.51}_{-1.38}) \times 10^{12}$	9.11×10^{01}	3.56×10^{02}	0	$(2.67^{+2.44}_{-1.68}) \times 10^{03}$	$(1.52^{+0.21}_{-0.21}) \times 10^{02}$	$(3.15^{+1.52}_{-1.39}) \times 10^{02}$
^{36}Ar	5.73×10^{15}	$(1.23^{+0.17}_{-0.17}) \times 10^{13}$	$(1.14^{+0.74}_{-0.58}) \times 10^{13}$	1.48×10^{04}	2.43×10^{04}	2 (0:59)	$(2.38^{+1.95}_{-1.38}) \times 10^{04}$	$(1.86^{+0.26}_{-0.26}) \times 10^{03}$	$(1.14^{+0.74}_{-0.58}) \times 10^{03}$
^{84}Kr	1.18×10^{14}	$(3.48^{+0.49}_{-0.49}) \times 10^{11}$	$(1.04^{+0.66}_{-0.52}) \times 10^{12}$	1.63×10^{03}	1.97×10^{03}	28 (0:71)	$(1.32^{+1.14}_{-0.79}) \times 10^{03}$	$(5.28^{+0.75}_{-0.75}) \times 10^{01}$	$(1.04^{+0.66}_{-0.52}) \times 10^{02}$
^{130}Xe	6.46×10^{11}	$(6.46^{+0.91}_{-0.91}) \times 10^{09}$	$(1.48^{+1.21}_{-0.86}) \times 10^{10}$	3.27×10^{01}	3.90×10^{01}	36 (0:73)	$(2.49^{+2.07}_{-1.45}) \times 10^{01}$	$(9.80^{+1.38}_{-1.38}) \times 10^{-01}$	$(1.48^{+1.21}_{-0.86}) \times 10^{00}$
H_2O	1.07×10^{23}	$(4.77^{+1.36}_{-1.36}) \times 10^{22}$	$(1.56^{+0.49}_{-0.67}) \times 10^{22}$	4.26×10^{13}	6.51×10^{13}	55 (50:59)	$(2.96^{+0.29}_{-0.29}) \times 10^{13}$	$(6.15^{+1.76}_{-1.76}) \times 10^{12}$	$(1.28^{+0.40}_{-0.55}) \times 10^{12}$
^{12}C	7.74×10^{21}	$(1.08^{+0.49}_{-0.41}) \times 10^{22}$	$(3.92^{+0.46}_{-0.46}) \times 10^{21}$	7.26×10^{12}	7.39×10^{12}	65 (61:69)	$(1.56^{+0.36}_{-0.36}) \times 10^{12}$	$(1.64^{+0.74}_{-0.62}) \times 10^{12}$	$(3.93^{+0.46}_{-0.46}) \times 10^{11}$
S	6.80×10^{20}	$(2.19^{+0.26}_{-0.23}) \times 10^{22}$	$(3.56^{+0.69}_{-0.37}) \times 10^{21}$	2.46×10^{12}	2.55×10^{12}	87	$(3.31^{+0.11}_{-0.11}) \times 10^{11}$	$(2.02^{+0.24}_{-0.21}) \times 10^{12}$	$(1.97^{+0.28}_{-0.28}) \times 10^{11}$
Cl	1.72×10^{21}	$(6.11^{+1.19}_{-1.19}) \times 10^{20}$	$(3.26^{+0.63}_{-0.63}) \times 10^{20}$	3.71×10^{11}	5.47×10^{11}	47 (30:64)	$(2.27^{+0.71}_{-0.71}) \times 10^{11}$	$(9.27^{+1.80}_{-1.80}) \times 10^{10}$	$(3.26^{+2.83}_{-2.83}) \times 10^{10}$
F	8.07×10^{20}	$(2.26^{+0.41}_{-0.41}) \times 10^{21}$	$(4.56^{+0.46}_{-0.46}) \times 10^{20}$	4.15×10^{11}	4.48×10^{11}	96 (94:97)	$(1.77^{+0.55}_{-0.55}) \times 10^{10}$	$(3.43^{+0.63}_{-0.63}) \times 10^{11}$	$(4.57^{+0.46}_{-0.46}) \times 10^{10}$
Br	2.18×10^{18}	$(7.59^{+2.20}_{-2.20}) \times 10^{17}$	$(4.05^{+1.17}_{-1.17}) \times 10^{17}$	1.34×10^{09}	1.58×10^{09}	66 (33:88)	$(5.27^{+5.12}_{-3.46}) \times 10^{08}$	$(1.15^{+0.33}_{-0.33}) \times 10^{08}$	$(4.06^{+1.17}_{-1.17}) \times 10^{07}$
I	1.48×10^{17}	$(1.02^{+0.55}_{-0.55}) \times 10^{16}$	$(5.46^{+2.93}_{-2.93}) \times 10^{15}$	2.61×10^{08}	4.57×10^{08}	76 (50:93)	$(6.59^{+7.26}_{-4.78}) \times 10^{07}$	$(1.55^{+0.83}_{-0.83}) \times 10^{06}$	$(5.47^{+2.94}_{-2.94}) \times 10^{05}$

Abbreviations: DMM, depleted mid-ocean ridge basalt mantle; MORB, mid-ocean ridge basalt; N/S, not subducted; OIB, oceanic island basalt; PLM, primitive lower mantle or plume mantle.

[a]Surface inventory: N (Cartigny & Marty 2013), noble gases (Ozima & Podosek 2002), H_2O (Lécuyer et al. 1998), C (Hirschmann & Dasgupta 2009), S (Chaussidon et al. 1989), halogens (Kendrick et al. 2013).

[b]Mantle inventories are directly derived from values reported in **Table 1**, assuming DMM = 90 wt% and PLM = 10 wt% of the bulk mantle.

[c]The flux in from the slab (with and without considering serpentinite contribution) is derived from the bulk slab composition (**Table 1**) and assumptions of subduction parameters reported in Section 2.1.

[d]Recycling efficiencies are calculated by dividing net ingassing fluxes by total initial influxes (from the bulk slab composition, including serpentine). Ranges of recycling efficiencies are given in parentheses.

[e]Net ingassing fluxes are derived by subtracting total arc outfluxes from total initial influxes.

[f]Arc outfluxes: N: computed from N/S by Hilton et al. (2002) and S outflux by Fischer (2008) and Shinohara (2013); noble gases: ^{3}He from S outflux and $^{3}He/S$ by Hilton et al. (2002) and Kagoshima et al. (2015), $^{3}He/^{36}Ar$ from Matsumoto et al. (2002) and Broadley et al. (2016), noble gas elemental ratios relative to ^{36}Ar from Holland & Ballentine (2006); H_2O: scaled on the H_2O content in primary arc magmas (Plank et al. 2013); C: CO_2 outflux from arc volcanoes determined from Fischer (2008) and Shinohara (2013)—see the main text for a discussion of the CO_2 outflux determined from the S outflux and CO_2/S of 2.6 ± 0.3 from Fischer et al. (2019); S: Fischer (2008) and Shinohara (2013); halogens: Cl by Fischer (2008) and Shinohara (2013), F from Cl outflux and F/Cl by Fischer (2008), Br and I from Cl outflux and Br/Cl and I/Cl by Pyle & Mather (2009).

[g]Outfluxes from the DMM and PLM are derived from concentrations reported in **Table 1**, an assumed constant degree of partial melting, partition coefficients, and magma production rates reported in the main text. Mantle outfluxes of S, H_2O, and halogens are not derived from gas measurements but computed by combining the S, H_2O, and halogen contents of MORB and OIB primary magmas with the respective rates of magma production. See the main text and the **Supplemental Spreadsheet** for further details regarding the assumptions.

Supplemental Material >

greatly, and there is no single representative sample of subducting crust and oceanic lithosphere. The AOC is largely heterogeneous, and the extent of its alteration during subduction is debated, which affects the bulk volatile concentrations in average oceanic crust (Section 2.2). Keeping these caveats in mind, we assume that a slab composition can be used together with typical subduction parameters to estimate the global volatile influx. This exercise requires the inferred rate of AOC subduction to be roughly equivalent to that of magma production at MORs (~20 km^3/year) (Section 4.1). In this framework, we consider 62,338 km of active MOR (and ~5,000 km of backarc basin) spreading at an average rate of 46.6 mm/year and an average ocean crustal thickness of 6.4 km (Le Voyer et al. 2019), balanced by 51,310 km of subduction zones, converging at 62.3 mm/year (i.e., ~20 km^3/year of AOC subducted) (Bird 2003). We assume sediments to be ~400 m thick (e.g., Plank & Langmuir 1998, Straub & Layne 2003) and a pure serpentinite layer of ~375 m (corresponding to an intermediate scenario between 5% serpentinization of the upper 6 km of lithospheric mantle and 15% serpentinization of the upper 3 km; see **Supplemental Text Section 2** for further justification) (Barnes & Straub 2010, John et al. 2011). Slab inventories (**Figure 1**) are presented in **Table 1**.

Serpentinization: process of oxidation whereby water and other volatiles are added to the crystal structure of minerals within ultramafic rocks

Forearc: in a convergent margin, it represents the region between the oceanic trench and volcanic arc, including the accretionary wedge

Supplemental Material >

2.2. Major Volatile Contents of Slab Components

Some volatiles (e.g., H_2O) are held within pore fluids and labile hydrous mineral phases, which may be expelled and fluxed to the surface beneath the shallow forearc (e.g., Saffer & Tobin 2011, Faccenda et al. 2012). Hence, only a small fraction of volatiles trapped in such nonstructural sites [i.e., as fluid inclusions in coarse-grained lithologies (e.g., gabbros in AOC) or at grain boundaries in fine-grained materials (e.g., altered lavas and serpentinites)] may be transported into the mantle. Volatile elements that are structurally bound within minerals (e.g., phyllosilicates, carbonates, amphibole, and serpentinite) are most likely to be efficiently recycled (**Supplemental Text Section 1**).

Structurally bound water concentrations within marine sediments vary from 5 to 15 wt%, with a weighted global mean of ~7.1 wt% (Plank 2014). Importantly, sediments are strongly enriched in N compared to other slab components (Li & Bebout 2005) and can have variable bulk contents (from hundreds to thousands of micrograms/grams; a best estimate of 424 μg/g is adopted here after Busigny et al. 2011) (**Table 1**). The bulk C content of marine sediments is variable between subduction zones [~0.3–8.0 wt% (e.g., Clift 2017)] and is controlled by the carbonate compensation depth, seafloor depth, and carbonate content (e.g., from redeposited turbidites), which vary principally as a function of latitude (Berner & Raiswell 1984). Our best estimate is taken at 2.6 wt% to match the ~60×10^{12} g/year C flux in subducting sediments (Plank 2014, Plank & Manning 2019). Likewise, the S content of marine sediments is variable [0.05–1.00 wt% (Berner & Raiswell 1984)]; however, no average value exists in the literature. Our best estimate is taken as the intermediate value of ~5,000 μg/g, with an uncertainty of basically ~100%. Measurements of halogen concentrations in bulk lithified marine sediments are limited and show a large range of values due to the variable presence of salt, organic material, and carbonate, which can greatly influence the total halogen concentrations in marine sediments (Muramatsu & Wedepohl 1998). Noble gas concentrations in sediments are from Matsuda & Nagao (1986) and Staudacher & Allègre (1988).

Most crustal alteration takes place near the ridge axis shortly after formation, although drill cores indicate that alteration continues as the crust ages (Johnson & Semyan 1994). The model of Jarrard (2003) remains the most commonly used model of ocean plate hydration, with ~4.0–6.5 wt% H_2O in the upper 600 m of ocean crust. Jarrard suggested ~1.8 wt% H_2O in the ~1.5-km-thick sheeted dike layer, while seismic wave speeds in the deeper gabbro layers of the crust indicate lower amounts of alteration and ~0.4 wt% H_2O (e.g., Carlson & Miller 2003). Here,

we adopt a weighted average of ~1 wt% H_2O for the AOC. Concerning N, Li et al. (2007) and Busigny et al. (2019) reported concentrations of 1.3–18.2 μg/g (average = 9.8 μg/g) in AOC, suggesting N enrichment during early stages of hydrothermal alteration at ridges. Carbon contents in AOC decrease with depth, with a bulk C content of 400–600 μg/g (the best estimate is ~500 μg/g) (Alt 2003, Plank & Manning 2019). The bulk S concentration of the AOC is considered to be greater than the S concentration in MORB of ~1,000 μg/g (e.g., Labidi & Cartigny 2016) as a consequence of S addition through exogenic (biogenic or hydrothermal) processes. For example, S-bearing minerals are deposited during interaction between seawater and the ocean crust, which can thereby inherit a positive seawater $\delta^{34}S$ isotope signature (Alt 1995). In order to represent the intake of S by the AOC, we assume 1,100 μg/g S for the bulk AOC (i.e., ~10% intake by the AOC relative to MORB), which is within error of previous estimates for the S content of AOC (690 ± 600 μg/g) (Alt 1995, Alt & Shanks 2011). Bulk halogen concentrations, also variable due to the heterogeneous nature of hydrothermal alteration, are compiled in **Table 1** and are from Chavrit et al. (2016), Zhang et al. (2017), Kendrick (2019a,b), and Barnes & Cisneros (2012). Noble gas concentrations in AOC are from Chavrit et al. (2016).

The oceanic lithospheric mantle may undergo significant hydration along fracture zones (McCaig et al. 2018) or during bend faulting prior to subduction (Ranero et al. 2003), but its water content is poorly constrained. Average H_2O, N, C, and S contents of pure seafloor serpentinite (typically lizardite +/− chrysotile) are 12–13 wt% (Ulmer & Trommsdorff 1995, Kendrick et al. 2013), 2.4 μg/g [from 1.3 to 4.5 μg/g (Halama et al. 2014)], 510 ± 360 μg/g (Alt et al. 2012), and 914 ± 733 μg/g (Alt et al. 2012), respectively. Serpentinites can have high concentrations of halogens, particularly chlorine, and halogen ratios have been used to determine fluid sources in seafloor (abyssal) serpentinites in the oceanic lithosphere, forearc (mantle wedge) serpentinites, and ophiolitic serpentinites (e.g., Barnes & Sharp 2006; John et al. 2011; Kendrick et al. 2011, 2013, 2018; Kobayashi et al. 2017; Cai et al. 2018). For example, high Br/Cl and I/Cl in forearc serpentinites suggest interaction with sedimentary and/or sedimentary-derived fluids (Kendrick et al. 2013, 2018, 2020; Kobayashi et al. 2017). Noble gas concentrations in serpentinite are from Kendrick et al. (2013).

3. VOLATILE RECYCLING EFFICIENCIES

When the slab subducts, a series of metamorphic reactions lead to incremental volatile release, with much of the plate's initial volatile budget returning back to Earth's surface through volcanic arcs (**Figure 1**; **Supplemental Figure 1**). To determine net ingassing fluxes, three approaches are typically adopted: (*a*) a mass-balance approach (Section 3.1), whereby total slab inputs (bulk slab concentrations; Section 2) are compared with outfluxes at volcanic arcs (with the difference assumed to be transported to the mantle) (e.g., Hilton et al. 2002); (*b*) a phase-equilibria approach, whereby thermodynamically derived phase assemblages and stoichiometric volatile concentrations are calculated for various subduction thermal fields (**Supplemental Text Section 1**) (e.g., Kerrick & Connolly 2001); and (*c*) an across-arc model, where volatiles are measured in forearc, arc, and backarc samples and then compared with known subduction inputs to assess how expelled slab fluids evolve as subduction progresses (Kendrick et al. 2020). Below we outline the constraints and caveats regarding volatile element behavior during subduction, calculate net ingassing fluxes and volatile recycling efficiencies, and explore the implications for our global mass-balance approach. Net ingassing fluxes are derived by subtracting total arc outfluxes from initial total influxes (from the bulk slab composition). Recycling efficiencies (%) are calculated by dividing net ingassing fluxes by total initial influxes. In the following, we consider our typical slab composition (best estimates, **Table 1**) for the subducting flux and only propagate uncertainties associated with outgassing fluxes to assess the global mass balance of each volatile.

Net ingassing flux: flux of volatiles that subduct past the arc, equal to total slab input fluxes upon subduction minus the total volcanic outfluxes at arcs

Supplemental Material >

Supplemental Material >

3.1. Previous Research

Arc volcanoes erupt more volatile-rich magmas than MOR or intraplate volcanoes, clearly implicating recycling of slab-derived fluids (e.g., Wallace 2005). One method to constrain arc outfluxes is to combine elemental ratios measured in arc volcanoes with SO_2 fluxes (Hilton et al. 2002, Fischer 2008, Kalacheva et al. 2018), as S is one of the few volatile elements that can be accurately measured using ground-based, airborne, and remote sensing methods (Galle et al. 2003). This approach may underestimate total S fluxes to the extent that S can be retained in the crust and fluxes associated with low-level degassing volcanoes are difficult to quantify (Fischer et al. 2019, Fischer & Aiuppa 2020), although ratios of degassed S to other elements should be reliable flux proxies. This approach can be challenging, however, due to large uncertainties associated with extrapolation of the derived fluxes over time, variations that occur over volcano eruption cycles, the lack of continuous time series data for most volcanoes, and difficulty with identification of nonatmosphere-influenced elemental ratios in volcanic gases (e.g., for N, which is abundant in the atmosphere relative to mantle reservoirs, and HNGs) (e.g., Hilton et al. 2002) (**Supplemental Text Section 3.1**).

Both Wallace (2005) and Fischer (2008) suggested that global H_2O outfluxes from arcs are approximately balanced with slab inputs. Output fluxes are, however, much better known than input fluxes due to inherent difficulties in sampling the material entering subduction zones and uncertainties associated with the extent alteration. Ruscitto et al. (2012) assumed a global magma flux of 1.4×10^8 kg/km/year and primary arc magma composition of 3.3 wt% H_2O (in good agreement with Plank et al. 2013) to suggest that 18–26% of subducted water erupts from arcs. However, these values are based on data from subaerial arcs and may need to be revised if quenched melt inclusions are unable to capture the primary water contents of some arc magmas (Fischer & Marty 2005, Wallace 2005, Gavrilenko et al. 2019, Krawczynski & Grove 2019), especially given that higher water contents are associated with magma varieties that are abundant in continental settings (Grove & Till 2019). The episodic nature of continental magma production rates (Ducea et al. 2015) is another major source of uncertainty, with recent estimates of island arc magma production rates (Jicha & Jagoutz 2015, Ratschbacher et al. 2019) up to 10 times larger than previous estimates. Higher magma production rates lead to higher estimates of arc H_2O outfluxes, which exceed combined inputs from sediments and AOC. While numerical models indicate that serpentinized lithosphere may not be a reliable candidate to close this mass balance (**Supplemental Text Section 1**), seismological (Grevemeyer et al. 2018) and direct observations of exhumed AOC from fault zones (McCaig et al. 2018) indicate the potential for additional AOC hydration during bend faulting, which could serve as an alternative mechanism to close this balance.

According to combined ^3He-CO_2 systematics, 10–20% of C emitted at arcs is derived from the mantle, with the remaining fraction originating from the slab (Sano & Williams 1996, Marty & Tolstikhin 1998). Kelemen & Manning (2015) reviewed C fluxes at subduction zones using compiled data, calculations of C solubility in aqueous fluids, and estimates of C flux in metasedimentary diapirs. In contrast to previous estimates (e.g., Gorman et al. 2006, Dasgupta & Hirschmann 2010), which suggested that about half of subducting C is recycled into the convecting mantle, these authors proposed a limited net transport of surface C to the mantle, although uncertainties were large and account for all or no recycled C. According to their study, most of the C released from the slab during subduction could remain sequestered in the mantle lithosphere, crust, and arc itself (Kelemen & Manning 2015). Notably, solid-state decarbonation reactions are ineffective until greater than 600°C (e.g., Kerrick & Connolly 2001), implying that C release from the slab is likely controlled by aqueous dissolution (e.g., Ague & Nicolescu 2014), which emphasizes how C and H_2O may be coupled under forearc conditions. A recent field-based study of dissolved and

gaseous CO_2 in Costa Rica (Barry et al. 2019) showed that significant C sequestration could also occur in forearc regions.

Previous mass-balance calculations suggest that the slab input of halogens is greater than the volcanic outflux at arcs, resulting in a net influx of halogens to the mantle (e.g., Barnes et al. 2018, Kendrick et al. 2020). Additional evidence for Cl recycling into the mantle has been proposed based on the similarity between Cl/K, Br/Cl, and I/Cl ratios and δ^{37}Cl values measured in arcs and subducting lithologies (e.g., Stroncik & Haase 2004; Workman et al. 2006; John et al. 2010; Kendrick et al. 2017, 2020). Likewise, HNG systematics in mantle-derived samples exhibit compelling evidence for the ubiquitous presence of surface-derived components in the solid Earth, with greater than or equal to 80% of mantle Xe originating from recycling (e.g., Holland & Ballentine 2006, Parai & Mukhopadhyay 2015). However, the respective recycling efficiencies of noble gases during subduction remain largely unknown.

Diffuse degassing: mantle- or slab-derived gases that percolate through Earth's crust over a wider area than point-source volcanic emissions

3.2. Volatile Mass Balance at Arcs

Here we adopt an internally consistent mass-balance model whereby volatile transfers affecting the surface inventory are defined as outflux from the depleted mid-ocean ridge basalt mantle (DMM) + outflux from the primitive lower mantle or plume mantle (PLM) − influx from subducting slabs + outflux from arcs. Our approach uses a unique magma production rate for each geological setting, balancing the rate of oceanic crust production at MOR with that of subducted AOC. MORB generation, subduction, and arc volcanism rates are tied to the plate boundary model of Bird (2003). We assume a total length of arc volcanism of 41,048 km by estimating the length of active volcanism that spans ~80% of trenches with active subduction (Bird 2003, Smithsonian Inst. 2013). We then use S fluxes (mol/km/year) estimated from remote and direct measurements of arc volcanic gas (Fischer 2008, Shinohara 2013, Carn et al. 2017) to derive total arc fluxes (**Table 2**). The volcanic SO_2 emission inventory derived from global satellite measurements suggests a total arc outflux of $\sim 7.51 \times 10^6$ mol S/km/year (Carn et al. 2017), in good agreement with commonly used S global outflux estimates from volcano measurements [$\sim 8 \times 10^6$ mol S/km/year (Fischer 2008, Shinohara 2013)], despite the latter being based on the obsolete hypothesis that the global S outflux distribution follows a power-law distribution (Mori et al. 2013, Carn et al. 2017). Here, H_2O, CO_2, and Cl fluxes are estimated based on their ratios to S in persistently degassing volcanoes following Fischer (2008) and Shinohara (2013). Note that the average CO_2/S used for arc volcanoes [2.6 ± 0.3 (Aiuppa et al. 2017, Fischer et al. 2019)] is actually lower than previously estimated values [~6 (Fischer 2008); ~3.5 (Shinohara 2013)]. As discussed in Section 5.3, the contribution of diffuse degassing to the global outflux of CO_2, and most likely other volatiles, is undoubtedly important, although largely underconstrained (Fischer et al. 2019, Werner et al. 2019). The ^{3}He and N fluxes are also determined based on their ratio to S (Hilton et al. 2002, Fischer 2008, Kagoshima et al. 2015). Our estimate of the N arc flux is an upper estimate, considering the total amount of N measured in arc volcanic gas, not only the fraction deriving from air-saturated water (Hilton et al. 2002). The F/Cl (Fischer 2008), Br/Cl, and I/Cl (Pyle & Mather 2009) of arc volcano gas data—which agree well with values derived from backarc glass analyses (Kendrick et al. 2020)—are used in combination with Cl fluxes to derive halogen fluxes. To date, estimates of the HNG outfluxes at arcs have been hampered by the absence of isotopic deviations from atmospheric compositions in arc volcanoes, precluding deconvolution of mantle, slab, and atmospheric signals. For this reason, previous estimates of the recycling efficiencies of noble gases [e.g., less than 5% for ^{36}Ar (Holland & Ballentine 2006)] have relied on comparisons between estimates of noble gas influxes and inventories of recycled noble gases in the present-day mantle. Here, our best estimates for the net influx of noble gases (**Table 2**) are tied to the ^{3}He

Supplemental Material >

Net ingassing state: slab influx (subduction)/global outflux (arcs + MOR + plume-related volcanism) > 1

fluxes, which are not significantly affected by air contamination, combined with elemental ratios of subduction-derived fluids from mantle xenoliths (**Supplemental Text Section 3.1**).

A second approach for estimating volatile outfluxes at arcs is to combine estimates of the primary magmatic volatile abundances from melt inclusions with magma production rates (e.g., Wallace 2005, Ruscitto et al. 2012, Plank et al. 2013), although this approach suffers from uncertainties in magma ascent pathways, magma mixing and assimilation, postentrapment loss of H_2O and CO_2 from melt inclusions (e.g., Moore et al. 2015), and arc magma generation rates (Section 3.1). To maintain consistency with the global mass balance and H_2O flux calculated via S outgassing ratios, an assumed average of 3.4 wt% H_2O in primary arc magmas (Plank et al. 2013) requires an arc magma production rate of 3.8×10^8 kg/km/year. Given the length of active arcs, this magma production rate corresponds to 125 km^3/km/Myr, which is ~4 times the rate assumed by Ruscitto et al. (2012) and Wallace (2005), although consistent with the higher rates proposed by Jicha & Jagoutz (2015) and Ratschbacher et al. (2019). This results in a total arc magma production of ~5 km^3/year, which is 25% of the MOR production rate and similar to the frequently cited 20% value of Crisp (1984). Given the above, the ^{3}He content of primary arc magmas is ~40% of MOR, and total CO_2 contents are up to 0.55 wt%, which is marginally lower than previous estimates from primitive undegassed subarc melts (Fischer & Marty 2005). Lower ^{3}He contents in arc magmas relative to MORB may be realistic, given that arcs likely have higher average extents of melting than MORB (Turner & Langmuir 2015) and that arcs with backarc spreading centers may be derived from peridotite that has undergone prior melt extraction (e.g., Tollstrup et al. 2010). Primary arc-magma halogen contents estimated using our approach are in remarkably good agreement with values reported from melt inclusion analysis and submarine glass data (Straub & Layne 2003, Kendrick et al. 2020).

In **Figure 2*a***, we show that all volatiles other than the light noble gases (He, Ne) are in a net ingassing state at arcs (i.e., slab influx/arc outflux greater than 1), suggesting that some amounts of these volatiles are transported past depths of arc-magma genesis (see **Supplemental Figure 2** for recycling efficiencies expressed in percent). The net ingassing states for Ar, Kr, and Xe are within error of unity (i.e., recycling efficiency equals 0%), but best estimates indicate net ingassing (greater than 1) at arcs for Kr and Xe, which is in good agreement with the occurrence of atmosphere-derived HNGs in the mantle (e.g., Holland & Ballentine 2006). We also find that ~40% of subducted water is returned to the surface at arcs (equaling 55% recycling efficiency). This result is consistent with recent thermomechanical models (**Supplemental Text Section 1**), which further suggest that an additional 25% of the subducted water may be lost in the forearc (a sink that is neglected in our approach). For N, a maximum of 62% of the N influx returns to the surface via arc volcanism (minimum 38% recycling efficiency). This is a conservative estimate and lower than previous estimates for the Izu-Bonin-Mariana margin, where Mitchell et al. (2010) estimated that 4–17% of N subducted in sediments and AOC is returned via arc volcanism (i.e., recycling efficiency equals 83–96%). A high recycling efficiency of N is in line with the fact that N is retained in high-pressure metasediments and peridotites to depths greater than 70 km due to NH_4 substitution for K in phengite (which is stable to ~300 km) or N_3^- ions substituting for oxygen (Watenphul et al. 2009, Cartigny & Marty 2013), with no significant loss of N by dehydration (Busigny et al. 2003, 2011; Halama et al. 2014) (see Section 5.3). As shown in **Figure 2*a***, F is likely decoupled from other halogens, suggesting a greater return of F into the mantle (e.g., Straub & Layne 2003). This decoupling could in part be due to the preferential incorporation of F over Cl in nominally anhydrous minerals [e.g., olivines, pyroxenes (Beyer et al. 2012, Dalou et al. 2012, Bernini et al. 2013, Fabbrizio et al. 2013)] and, more generally, to the low solubility of F relative to other halogens in surface water (e.g., Kendrick et al. 2020). In **Figure 2*b***, we plot influx/surface inventory ratios and normalize all volatile species to N to visualize the impact of

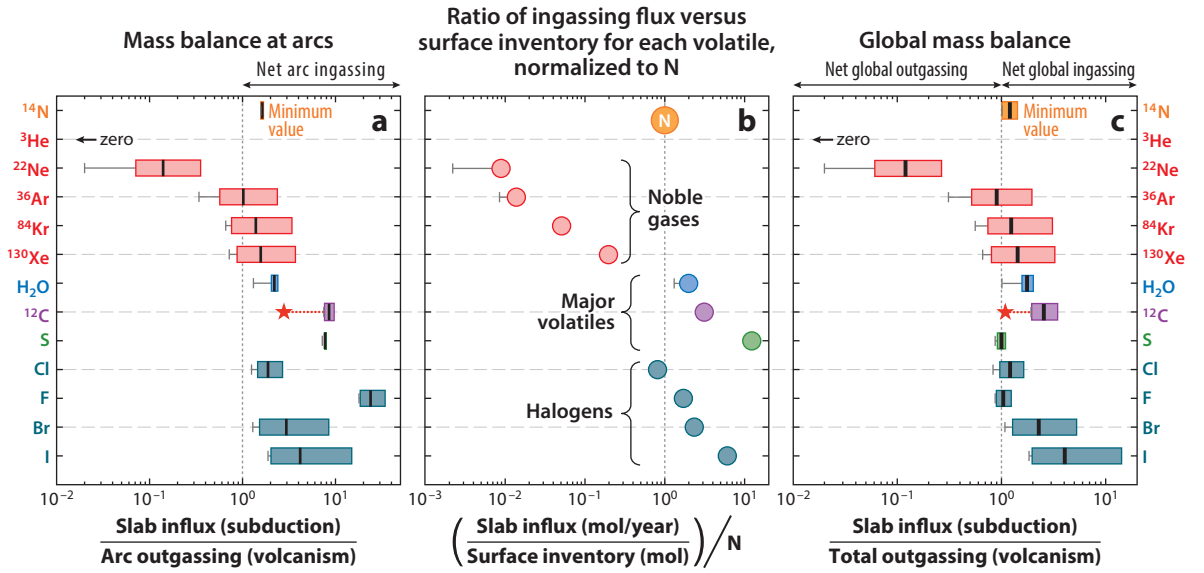

Figure 2

(*a*) Volatile ingassing flux from the slab (i.e., sediments + AOC + serpentinized lithospheric mantle) relative to the outflux from volcanic arcs. (*b*) The ingassing flux versus surface inventory (i.e., mol/year input by the slab relative to the total mols in surface reservoirs) normalized to N. (*c*) Volatile ingassing fluxes from the slab relative to the total volatile outfluxes (i.e., arcs + MORB + PLM). Uncertainties are shown as colored horizontal bars in panels *a* and *c*. Gray bars extending to the left side of each data point refer to a minimum slab input estimate corresponding to slab compositions with no serpentinite considered. Note that the N outflux at arcs is considered a maximum value (Section 3.2), so the estimates reported in panels *a* and *c* for N are minimum values. Red stars in panels *a* and *c* represent our best estimates for C when considering the potential effect of diffuse degassing (Fischer et al. 2019, Werner et al. 2019). Note that uncertainties on the mass balance of S are virtually small due to the fact that uncertainties associated with the slab influx, which would be very large for S (on the order of 100%; Section 2.2), are not propagated (only best estimates are being used for slab influxes; **Table 1**). Abbreviations: AOC, altered oceanic crust; MORB, mid-ocean ridge basalt; PLM, primitive lower mantle or plume mantle.

recycling on volatile surface inventories. It becomes clear that, compared to N, significant fractions of H_2O, C, S, and halogens are subducted relative to their respective surface inventories. However, the surface C inventory is relatively small compared to other major volatiles (H_2O, N) (**Table 2**), so C recycling has a greater impact on the surface inventory than do H_2O and N, as was recently noted by Hirschmann (2018) (**Figure 2*b***).

4. MANTLE RESERVOIRS: VOLATILE INVENTORIES AND OUTFLUXES

Once transported past volcanic arcs, volatiles are ultimately incorporated into Earth's mantle. Quantifying volatile concentrations in mantle reservoirs is important to determine the overall extent of volatile recycling. Estimating the mantle concentrations of volatiles with low solubilities in mantle-derived melts is challenging because C, N, and noble gases are always partially degassed and thus fractionated from one another during magma ascent and/or eruption (e.g., Holloway & Jakobsson 1986, Jambon 1994), unlike H_2O and halogens, which are retained in submarine basalts. The volatile content of mantle reservoirs is therefore estimated from their concentrations in the least degassed lavas. Primary magma compositions are either derived indirectly, from ^{3}He fluxes, volatile elemental ratios, and magma production rates (Marty 2012), or measured directly in undegassed basalts or melt inclusions and scaled to a better constrained lithophile element with

similar compatibility (e.g., Ba or Nb for CO_2) (Saal et al. 2002, Cartigny et al. 2008, Michael & Graham 2015).

Estimating mantle volatile concentrations is complicated by the fact that the mantle is heterogeneous and not all reservoirs are well sampled [e.g., the SCLM and transition zone (**Supplemental Text Section 6**)]. Further, basalts erupted at ridges and ocean islands sample additional chemical and isotopic mantle heterogeneities [i.e., normal-type MORB, enriched-type MORB, enriched mantle 1, enriched mantle 2, high μ mantle domain, FOcus ZOne (Allègre 1982, Zindler & Hart 1986, White 2010)] with distinct volatile elemental and isotopic characteristics that are considered to result from variable recycled crustal contributions, potentially distinct primordial materials, and different degassing/mixing histories. For the sake of simplicity, we consider here the two main mantle reservoirs: the DMM sampled by MOR volcanism, which we consider broadly representative of the convecting mantle, and the high $^3He/^4He$ PLM, which represents the least degassed portions of the deep Earth. We note that the size, location, and composition of the deep reservoir(s) sampled by mantle plumes are poorly constrained. From a seismological and mineralogical point of view, the upper (30 vol%) and lower (70 vol%) mantle are delineated by the transition zone. However, the abundance of radiogenic ^{40}Ar in the atmosphere indicates that at least 50% of the mantle is degassed (Allègre et al. 1996). The volume of the PLM source (i.e., the least modified and least degassed reservoir that feeds hotspot volcanism) is probably best represented by large low-shear-velocity provinces (LLSVPs), which are denser than the rest of the mantle and thus less prone to homogenization via convection (e.g., Zhang et al. 2016, Parai et al. 2019). LLSVP structures may account for ~8 vol% of the total mantle (Cottaar & Lekic 2016), and we assume here that they represent the PLM reservoir. We take DMM and PLM to be 90 wt% and 10 wt% of the bulk mantle, respectively. Our estimates of their volatile inventories are reported in **Table 2** and explained in detail below. Mantle outfluxes of C and noble gases are computed directly from ^3He outfluxes. We then use our calculated ^{36}Ar flux to derive the outflux of N. H_2O, S, and halogen outfluxes are derived from mantle concentration estimates (see a compilation of mantle halogen contents in **Supplemental Table 2**). For both the DMM and PLM, volatile concentrations and outfluxes are related by a unique degree of partial melting (11% and 9% for the DMM and PLM, respectively) and magma production rate (20 km^3/year and 1.21 km^3/year, respectively).

Supplemental Material >

Transition zone: ultramafic and peridotitic region of Earth's mantle located between the lower mantle and the upper mantle at depths of 410–660 km

Large low-shear-velocity province (LLSVP): located within the lowermost mantle and characterized by slow shear wave velocities; sometimes referred to as a superplume

Popping rock: volatile-rich basalt from the Mid-Atlantic Ridge that often pops or explodes upon being brought to the surface

4.1. Depleted Mid-Ocean Ridge Basalt Mantle

To determine the volatile inventory of the DMM, we assume a MOR magma production rate of ~20 km^3/year (**Supplemental Material**) and an 11% degree of mantle partial melting on average. The MOR ^3He flux has been recently revised using a data-assimilated deep ocean circulation model, yielding a range of 640–850 mol ^3He/year (Holzer et al. 2017). MOR fluxes and DMM abundances of noble gases are then estimated by using noble gas elemental ratios measured in popping rocks (Moreira et al. 1998). Based on the $C/^3He$ of the MORB mantle (Javoy & Pineau 1991, Marty & Zimmermann 1999, Resing et al. 2004), the C flux at MOR is estimated to be $1.6 \pm 0.6 \times 10^{12}$ mol C/year, which is in excellent agreement with the flux estimated by Le Voyer et al. (2019), who extrapolated from undegassed MORB samples to the global ridge system. While our total flux is ~20% higher, it includes the longer estimate of Bird (2003) for the total length of spreading ridges, in which backarc basin (BAB) basalts are considered as part of the MOR system. Given that BAB magmas have higher primary C compared to MORBs (e.g., Mattey et al. 1984), our C flux should be considered a minimum. Our estimate of ridge C flux also overlaps with that of Hirschmann (2018), who provided a comprehensive compilation of recent ridge C flux estimates. The C content of primary MORB magma derived from our C flux

estimate and magma production rate is 37 ± 20 μg/g, which is within error of estimates of the DMM C content based on the Siqueiros melt inclusions [19 ± 5 μg/g (Saal et al. 2002)] or the estimate of 16 ± 9 μg/g by Salters & Stracke (2004).

The behavior of N during partial melting is not well constrained (Javoy & Pineau 1991, Mikhail & Sverjensky 2014). However, assuming similar behaviors for N and ^{36}Ar during degassing, and given that the K/N ratio of the mantle appears indistinguishable from that of the continental crust, Marty & Dauphas (2003) suggested N behaves as an incompatible element. Here, we use the N/^{36}Ar of Marty & Dauphas (2003) and a ^{36}Ar content derived from ^{3}He to compute the N content of the DMM source. We find a range of 0.21–0.69 μg/g N, with a best estimate of ~0.40 μg/g (**Table 1**), which is within error of the estimate previously derived by Marty & Dauphas (2003) (0.27 ± 0.16 μg/g) but notably lower than the convecting mantle value of 1.10 ± 0.55 μg/g used by Hirschmann (2018) (which corresponds to the bulk mantle content).

Water is more soluble than CO_2 and noble gases in magma at low pressures, so the abundance of H_2O in the DMM source can be directly estimated from measurements of H_2O in MORB glasses, erupted at water depths of 2,000–3,000 m, therefore retaining their initial H_2O. Here, we adopt the DMM water content derived by Le Voyer et al. (2017) (238 ± 68 μg/g), which is significantly higher than previous estimates [150 ± 50 μg/g (Dixon et al. 2002, Saal et al. 2002, Salters & Stracke 2004, Le Roux et al. 2006, Clog et al. 2013)] but in good agreement with recent values derived by Hirschmann (2018) from H_2O/Ce and CO_2/Ba of oceanic basalts (290 ± 80 μg/g). Interestingly, combining 238 μg/g H_2O in the DMM source with the H/C mass ratio of 0.75 derived by Hirschmann & Dasgupta (2009) gives a C content of the MORB mantle source of 35 μg/g, in excellent agreement with the C content derived from the C/^{3}He of the MORB mantle (37 ± 20 μg/g). The H_2O content of MORB primary magma (1,836 μg/g) is then computed using the batch melting equation and partition coefficient of Ce [0.022 (Workman & Hart 2005)], assumed to be the same as that of H_2O (Le Voyer et al. 2017).

The flux of S from the DMM is estimated by combining typical S concentrations in MORBs [1,000 ± 50 μg/g (Labidi & Cartigny 2016)] with the total flux of basalt emitted at MOR (~20 km^3/year) (yielding the amount of S entering the oceanic crust). Kagoshima et al. (2015) used S/^{3}He in MORB vesicles to show that a fraction of S emitted at MOR is degassed. Comparing the potential flux of degassed S [estimated from the ^{3}He MOR flux (Holzer et al. 2017) and S/^{3}He in MORB glass vesicles (Kagoshima et al. 2015)] with the flux of undegassed S [computed from the S content of MORBs (Labidi & Cartigny 2016) and MORB magma production rate], we find that greater than 93% of the S emitted at MOR would remain in the magma, where it solidifies as sulphides in the MOR crust and does not contribute to the MOR flux that discharges into the ocean and atmosphere. The S content of the DMM is taken to be 195 μg/g (Nielsen et al. 2014). Halogens are not degassed from basalts erupted at water depths greater than 500 m (Unni & Schilling 1978). Considering that the average depth of MORs is 2,500 m (Parsons & Sclater 1977), the degassing flux of halogens during oceanic crust formation is considered to be negligible. The abundance of F and Cl in the DMM can therefore be determined by comparison with a lithophile element of similar mantle incompatibility, in this case F/Pr and Cl/K (Kendrick et al. 2017) (**Supplemental Table 2**). Coupling the F/Pr (108 ± 2) and Cl/K (0.06 ± 0.01) measured in MORB glasses (Kendrick et al. 2017) with mantle concentration of Pr [0.11 ± 0.02 (Workman & Hart 2005)] and K [100 ± 10 (Arevalo et al. 2009)], we then calculate the F and Cl concentrations of the DMM to be 12 ± 2 μg/g and 6 ± 1 μg/g, respectively (**Supplemental Table 2**). Concentrations of Br and I are then calculated using the DMM Cl concentration together with the Br/Cl and I/Cl of MORB glasses as determined by Kendrick et al. (2017) (**Table 1**).

Supplemental Material >

4.2. Plume Mantle

Assessing the global outflux of volatile elements from the PLM is particularly challenging due to inherent uncertainties in the volatile inventory, magma production rate, and degree of partial melting associated with the PLM, as well as in the quantification of global outfluxes from this reservoir. Based on the annual production of oceanic island basalt (OIB) versus MORB lavas, it is likely much lower than MOR fluxes, such that the PLM has remained relatively undegassed (Mukhopadhyay 2012). The plume-associated magma production rate has been estimated to range from 0.1 to 2.5 km^3/year for intracontinental and 1.8 to 2.4 km^3/year for intraoceanic settings (Crisp 1984). Uncertainties are large due to the episodic nature of plume-related volcanism, and thus plume-associated magma production could represent 1–12% of MORB production (Porcelli & Ballentine 2002). In addition, because the flux of ^{3}He from intraplate volcanic systems is dominantly subaerial, it is not possible to directly obtain a time-integrated value (Porcelli & Ballentine 2002). Estimates for the PLM volatile inventory and outgassing flux must therefore be taken with caution.

Gonnermann & Mukhopadhyay (2007, 2009) proposed a model of nonequilibrium degassing and mixing between primordial and recycled noble gases to propose a ^{3}He content in the PLM within the range $(1.37–3.28) \times 10^{-14}$ mol ^{3}He/g. This is 10–24 times higher than the ^{3}He content of the DMM, in excellent agreement with the factor of 15 proposed by Hilton et al. (2000) from He-Pb systematics along the Reykjanes Ridge. Here, this range of ^{3}He in the PLM is combined with an intraplate magma production rate of 1.21 km^3/year (i.e., 6% of MOR) and a 9% degree of mantle partial melting to yield a global PLM ^{3}He flux of 551–1,320 mol/year, which overlaps with previous estimates by Porcelli & Ballentine (2002) (38–670 mol ^{3}He/year). Noble gas outfluxes from the PLM are scaled to this ^{3}He range by using the elemental ratios measured in Icelandic [for Ne, Ar, Xe (Mukhopadhyay 2012)] and Réunion [for Kr (Trieloff et al. 2002, as this element was not analyzed by Mukhopadhyay 2012)] volcanoes. The large assumptions and uncertainties associated with the PLM ^{3}He flux preclude a straightforward determination of the N and C outfluxes from the PLM. On the basis of the N_2–Ar systematics in high ^{3}He/^{4}He samples, the PLM N content has been estimated to be ~2.7 ± 1.4 μg/g (Marty & Dauphas 2003), although a recent re-evaluation of N_2–^{36}Ar systematics of the ^{3}He-rich plume Yellowstone suggests that this value could be as high as ~30 μg/g (Labidi et al. 2020). Importantly, a significant fraction of N in the PLM source could be derived from recycling (see **Supplemental Text Section 4** and Section 5.3 for discussion). Here, we combine the PLM N content derived by Marty & Dauphas (2003) with the estimated flux of PLM magma and degree of partial melting to derive a N flux from the PLM (~7.8×10^9 mol N/year; **Table 2**).

The C content scaled to the ^{3}He flux and inferred C/^{3}He of the PLM [3×10^9 (Marty & Tolstikhin 1998)] is markedly higher (498–1,192 μg/g) than previous C plume source estimates [~13 μg/g (Barry et al. 2014, using CO_2 concentrations in Icelandic basalts), 100–130 μg/g (Tucker et al. 2019, from the analysis of OIB melt inclusions), and 370 μg/g (Miller et al. 2019, from CO_2/Ba and CO_2/Nb in melt inclusions from the Iceland plume olivine)]. This suggests that the C/^{3}He of the PLM is poorly known, so we consider the value by Tucker et al. (2019) to be our best estimate. The H_2O and S outfluxes are computed from the estimated flux of PLM magma (1.21 km^3/year), combined with primary magmatic content in OIBs. Based on H_2O/Ce ratios measured in the Loihi Seamount, Dixon & Clague (2001) estimated the PLM source H_2O concentration to be 400 ± 30 μg/g, similar to values reported by Wallace (1998) from the analysis of OIBs in Kilauea (450 ± 190 μg/g H_2O). These estimates are, however, much lower than values determined for the Iceland plume source [from 620–920 μg/g (Nichols et al. 2002) up to ~9,400 μg/g (Hallis et al. 2015)]. Here we adopt the intermediate value of ~700 μg/g

Supplemental Material >

H_2O proposed by Simons et al. (2002) for the PLM. An S content of 1,500–2,000 μg/g in OIB is considered for estimating the S outflux (Labidi et al. 2015, Lorand & Luguet 2016). The halogen concentrations of the PLM are determined in a way similar to that of the DMM, using the F/Pr and Cl/K measured in OIB glasses, which are indistinguishable from that measured in MORB glasses (Kendrick et al. 2017) (**Supplemental Table 2**). Taking the measured Pr and modeled K concentrations of the PLM to be 0.20 ± 0.02 μg/g (Jackson & Jellinek 2013) and 480 μg/g (Arevalo et al. 2009), we calculate the PLM to have F and Cl concentrations of 22 ± 2 μg/g and 29 ± 6 μg/g, respectively (**Supplemental Table 2**). These values are remarkably consistent with the values given by Kendrick et al. (2017), which were calculated by summing the abundances of F and Cl in the main terrestrial reservoirs and assuming it was originally present in the PLM. Recent research on halogens in glasses from the Samoa, Pitcairn, and Society plumes shows Br/Cl and I/Cl similar to that of MORB, suggesting the two reservoirs are well mixed and may share a similar subducted halogen origin (Kendrick et al. 2014, 2015, 2017) or require no subduction. The Br/Cl and I/Cl from Kendrick et al. (2015, 2017) are again used to derive the Br and I contents of the PLM.

Supplemental Material >

5. EVOLUTION OF THE VOLATILE BUDGET OF EARTH'S RESERVOIRS

All volatile elements apart from He and Ne are estimated to currently be in a net ingassing state at arcs (**Figure 2*a***; Section 3), implying that they are transported from the surface to mantle reservoirs [see recycling efficiencies (%) in **Table 2**]. Net ingassing fluxes can then be considered alongside PLM and DMM outgassing fluxes to determine the solid Earth's modern net ingassing/outgassing state for each volatile element (**Figure 2*c***). Extrapolating these values from present-day reservoirs provides constraints on the past volatile evolution of Earth's surface (**Figure 3*b***). To address uncertainties related to (*a*) when cold subduction, capable of volatile recycling, began and (*b*) how past recycling efficiencies evolved through time, we developed a box model that uses N contents and isotopes in terrestrial reservoirs to constrain the history of N recycling through time (after Barry & Hilton 2016, Labidi et al. 2020). We discuss the implications of this approach within the context of past surface volatile inventories.

5.1. Net Ingassing/Outgassing: A Global Mass Balance

In **Figure 2*c***, we normalize all influx best estimates to total outflux best estimates (from arcs, DMM, and PLM) to infer the modern global ingassing/outgassing state of each volatile element. We observe that N, H_2O, C, Cl, Br, and I appear in a net ingassing state, suggesting that their respective surface inventories may be decreasing with time. For C, we observe that taking into account the potential effect of diffuse degassing (Fischer et al. 2019; **Figure 2*c***) brings the C ingassing/outgassing balance close to steady state (i.e., global ingassing/outgassing ∼1). Likewise, Ar, Kr, Xe, S, and F appear close to steady state, but best estimates for Kr and Xe suggest they are also in a net ingassing regime. Conversely, Ne appears in a net outgassing regime, suggesting that the surface inventory of Ne is increasing through time. However, whether the present-day mass balance can be used to reconstruct the past evolution of surface-mantle interactions remains in question. For example, Parai & Mukhopadhyay (2018) showed that substantial recycling of atmospheric Xe into the deep Earth could not have occurred before 2.5 Ga and that the net ingassing of Xe became significant only during the past 1 Gyr. Because hydrous minerals carry Xe during subduction, the authors argue that H_2O and Xe are coupled during subduction, which implies that the recycling efficiencies of both H_2O and Xe would have increased through time. However, there is also the potential for H_2O and noble gases to be decoupled from one another during

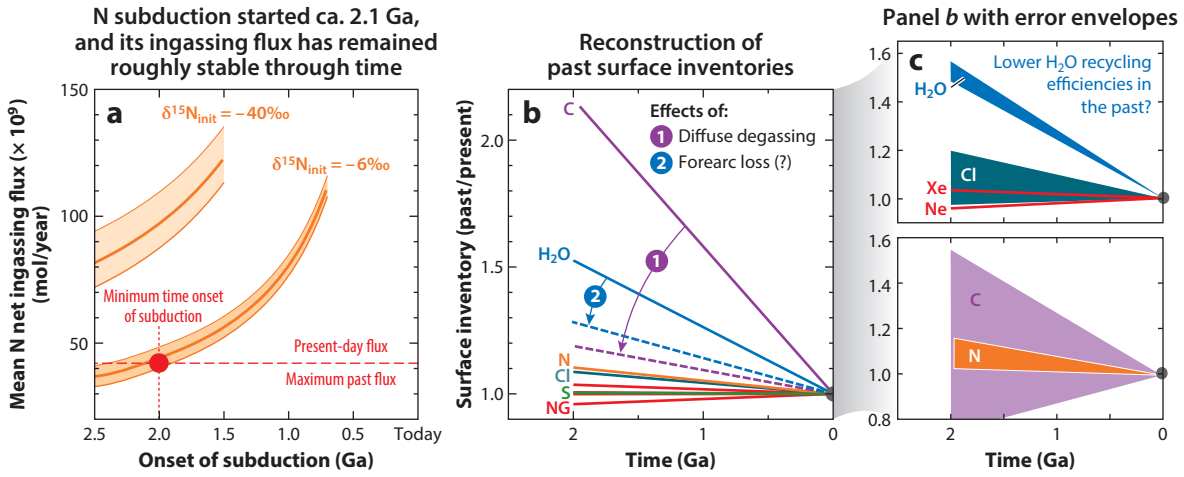

Figure 3

Reconstruction of the past surface inventory of volatile elements. Panel *a* shows the outcomes of our box model that satisfy N isotopic and elemental evolution in surface and mantle reservoirs (**Supplemental Text Section 4**). We plot mean N net ingassing flux as a function of subduction duration (the error envelopes correspond to the propagation of uncertainties on outfluxes from the PLM and DMM). Assuming an initial $\delta^{15}N$ at −6‰ for the bulk mantle (Labidi et al. 2020), the model required past N net ingassing fluxes to have been equal to, or lower than, present-day estimates (~42 × 10^9 mol/year; **Supplemental Figure 3**), suggesting that efficient N recycling started ca. 2 Ga. If N recycling began between 2.0 and 2.5 Ga, the model predicts marginally lower net N ingassing fluxes in the past relative to present, suggesting that N recycling efficiency has remained roughly constant through time. Panel *b* shows the surface inventory evolution, calculated using the modern ingassing/outgassing states for each element, which are assumed to have remained constant through time (*solid lines*). The purple dashed line corresponds to the surface-inventory evolution of C, taking into account diffuse degassing from the mantle (Plank & Manning 2019). The blue dashed line represents the surface inventory evolution of H_2O if a significant fraction (up to ~25%) of water in the slab were lost to the forearc, as predicted by thermomechanical models of slab dehydration during subduction (**Supplemental Text Section 1**; Section 5.3). Panel *c* displays the same evolution of the surface inventory as presented in panel *b* but showing error envelopes associated with uncertainties in our determination of total outfluxes from the mantle. Abbreviations: DMM, depleted mid-ocean ridge basalt mantle; NG, noble gas; PLM, primitive lower mantle or plume mantle.

subduction, with H_2O being progressively lost from minerals via H^+ diffusion and noble gases potentially reaching the lower mantle in anhydrous slabs (Kendrick et al. 2013). Here, we use a box model of N recycling through time (**Figure 3*a***) to test whether the present-day mass balance can be used to reconstruct past surface inventories of all the volatile elements discussed in this contribution.

5.2. Nitrogen Model and Implications for Past Ingassing/Outgassing State of Earth

Nitrogen has emerged as a useful tool for exploring the secular evolution of volatile recycling because there are isotopic and concentration constraints for both surface (e.g., atmosphere, slabs) and mantle (PLM and DMM) reservoirs. Here, we construct a three-box model (atmosphere, DMM, and PLM) that investigates the fate of subducted N into mantle reservoirs and predicts the isotopic evolution of mantle and surface reservoirs since the onset of N subduction (**Figure 3*a***; taken from 0.7–2.5 Ga). In this model, N outfluxes from the PLM and DMM are considered to have remained constant through geological time (i.e., similar to present-day estimates). We then test the hypothesis that the heavy $\delta^{15}N$ of the PLM [+3‰ (Marty & Dauphas 2003)] and light $\delta^{15}N$ of the DMM [−5‰ (Javoy & Pineau 1991, Cartigny et al. 2014)] reflect progressive addition of subducted sedimentary material [$\delta^{15}N = +5$‰ (Li et al. 2014)] to an initially ^{15}N-depleted mantle.

Although N isotope compositions as light as −40‰ have been reported in deep-mantle diamonds, interpreted to reflect relict primordial nitrogen (Palot et al. 2012), such a light $\delta^{15}N$ starting mantle composition appears in conflict with several geochemical observations (**Supplemental Text Section 4**). Here, an initial value of −6‰ is assumed for the bulk mantle (after Labidi et al. 2020). This value is intermediate between $\delta^{15}N$ of ordinary (∼0‰) and enstatite (−30 ± 10‰) chondrites and may represent accretionary material from the inner Solar System (e.g., Javoy et al. 2010, Dauphas 2017) but excludes carbonaceous chondrites [$\delta^{15}N \sim +40$‰ (Alexander et al. 2012)] as the primary source of N in the primitive mantle. These assumptions do not consider the potential effect of N isotope fractionation during core formation (e.g., Dalou et al. 2019), which suggests that a direct parallel between the initial $\delta^{15}N$ of the mantle and Earth's accretionary materials may not be straightforward.

Supplemental Material >

Archean eon: one of the four geological eons of Earth's history, occurring between 4.0 and 2.5 Ga

If the onset of cold subduction occurred within the past 2 Gyr, our N box model would predict higher net N ingassing fluxes compared to present-day estimates. However, early volatile subduction is suggested to have been less efficient than at present due to the secular cooling of the mantle (Brown 2006). Nitrogen net ingassing fluxes for subduction durations greater than or equal to 2 Gyr broadly agree with present-day flux estimates (**Figure 2*a***; **Table 2**; Section 3), which suggests that (*a*) the onset of efficient transport of N to the mantle likely started before 2 Ga, in line with N isotopes in lithospheric diamonds indicating N subduction in the Archean eon (Smart et al. 2016), and that (*b*) its recycling efficiency remained roughly constant through geological time. Importantly, any scenario with an initial $\delta^{15}N$ at −40‰ for the bulk mantle (Barry & Hilton 2016) requires higher past ingassing fluxes of N than at present, which is unlikely, further indicating that the initial bulk mantle must have been more ^{15}N-rich than $\delta^{15}N = -40$‰ (**Supplemental Table 1**). Assuming subduction initiation at 2 Ga ($\delta^{15}N$ initial at −6‰), our model predicts that the total inventory of N and $\delta^{15}N$ of Earth's surface prior to the onset of subduction was at most 10% and approximately +1.8‰ greater than at present, respectively (**Supplemental Table 1**). This is broadly consistent with the sedimentary $\delta^{15}N$ record (Ader et al. 2016) and analyses of N in fluid inclusions trapped in Archean hydrothermal quartz (Marty et al. 2013, Avice et al. 2018), which indicates that the partial pressure and isotopic composition of atmospheric N_2 before 2 Ga were broadly similar to those of today. The model also predicts that the DMM has been in a net outgassing regime (presubduction N ∼20% > present), while the PLM has been in net ingassing (presubduction N ∼80% < present) (**Supplemental Table 1**). Additionally, the model predicts that ∼86% of N subducted to the mantle has been incorporated into the PLM (versus ∼14% into the DMM; **Supplemental Text Section 3**; **Supplemental Table 1**). This implied discrepancy in the fate of subducted N (Barry & Hilton 2016) appears to be in contrast with halogen (Kendrick et al. 2014, 2017) and noble gas (Broadley et al. 2020) data, which suggest similar amounts of recycled volatiles end up in the DMM and PLM. This discrepancy implies that N and H_2O-Xe halogens are transported into the mantle in distinct mineral phases (N chemical fixation into potassic minerals versus physical volatile trapping into hydrous mineral phases) that could induce decoupling of their behaviors during subduction (Section 5.3). Alternatively, the higher contents of primordial volatiles (e.g., noble gases) in the PLM relative to the DMM (Gonnermann & Mukhopadhyay 2007) suggest that greater amounts of surface-derived volatiles may need to be recycled into the PLM to reach a similar recycled-to-primordial ratio in the DMM, in agreement with the N model. Understanding the processes that would allow for most subducted N to reach the PLM, with limited contribution to the DMM, represents a critical avenue of future investigation (Busigny & Bebout 2013).

This isotope-driven model relies solely on the flux of sedimentary (^{15}N-rich) N and does not consider the flux of N from AOC, which could be significant but is poorly characterized for $\delta^{15}N$ [with values ranging from roughly −10 to +10‰ (Li et al. 2019)]. More research is required to

understand the potential controls of biological and geological processes [e.g., subduction erosion (von Huene et al. 2004)] on the relative contributions of sediments versus AOC to total subducted N and how these would have varied through geological time. Overall, adding the AOC contribution to our N isotope model (e.g., Li & Bebout 2005, Mitchell et al. 2010) would result in even greater estimates of past subducting N fluxes, therefore strengthening our interpretations that (*a*) past N subduction influxes were likely similar to (i.e., not significantly lower than) those of today and that (*b*) N subduction most likely started before 2 Ga (**Figure 2*a***). Lastly, our model is sensitive to the assumed thickness of sediments [~400 m (Plank & Langmuir 1998)], which could have varied over geological time. Present-day estimates of the mean global sediment thickness may be as high as ~530 m (Plank 2014), which would yield a present-day N net ingassing flux of $\sim 63 \times 10^9$ mol/year, corresponding to an onset of N subduction greater than or equal to 1.4 Ga (**Figure 3*a***; **Supplemental Text Section 4.2**; **Supplemental Figure 4**). Our model also neglects secondary processes potentially affecting the slab's budget of sediments past the arc [e.g., sediment diapirism (Behn et al. 2011)], which may ultimately reduce the efficiency of volatile transport into the deep mantle.

Supplemental Material >

5.3. Reconstructing Past Surface Volatile Inventories

To reconstruct the past evolution of Earth's surface volatile inventory, we first consider the present-day global ingassing/outgassing state of each volatile. We then combine the present-day budget at Earth's surface to back-calculate the past composition of Earth's surface volatile inventory assuming that this balance and fundamental subduction parameters (e.g., plate tectonic speed, mantle temperature) have remained roughly constant over the past 2.5 Gyr. We emphasize that our model assumes constant magma production and volatile degassing rates at MOR, which potentially varied by a factor greater than or equal to 3 over geological time (e.g., Li et al. 2016). Increasing the magma production rate at MOR would proportionally increase the rate of subducting AOC. Hence, the exact outcome of increasing MOR magma production rates on the global balance of volatile recycling is ultimately unknown.

We observe that the surface inventories of N, S, Cl, and noble gases would have remained relatively constant through time (**Figure 3*b***), in line with their respective input to total output (i.e., arcs + MORB + PLM) flux ratios being close to unity (**Figure 2*c***). A roughly constant partial pressure of atmospheric N_2 through time appears in agreement with the geological record (Marty et al. 2013, Avice et al. 2018), further suggesting that the ingassing rate of N must have been roughly constant since the onset of modern subduction (**Figure 3*b***). Conversely, the surface inventories of H_2O and C would have been significantly higher in the past (net ingassing regime). For C, this outcome is at odds with previous models by Kelemen & Manning (2015), who suggested that the C content of Earth's surface is increasing through time. This discrepancy is in part related to our model input for C influx from subducting sediments (Plank & Manning 2019), which is higher than that of Kelemen & Manning (2015), and shifts the present-day C flux balance to a net ingassing state. Importantly, considering C diffuse degassing from soils, springs and hydrothermal systems could potentially triple the estimate of C outflux at arcs and double the global estimate of C outflux (Fischer et al. 2019, Plank & Manning 2019, Werner et al. 2019, Fischer & Aiuppa 2020). Taking into consideration diffuse degassing suggests that the surface inventory of C could have remained roughly constant through time (**Figure 3*b***), in line with C being in a nearly balanced state of ingassing/outgassing (**Figure 2*c***). Past C and S surface inventories estimates, however, remain largely uncertain. Better estimating C and S outfluxes from the mantle requires extrapolating available data to unmeasured volcanoes, considering fluxes from all types of emitters, including explosive and diffuse degassing (which are particularly difficult to quantify), as well

as correcting for background biogenic sources (Fischer et al. 2019). In addition, the present-day global mass balance of S relies on our knowledge of the S content of the AOC, which is poorly known due to inherent difficulties in assessing the contribution from massive hydrothermal sulfide deposits that are added to the crust during hydrothermal alteration (Alt 1995).

Higher surface inventories of H_2O (+50%) and Cl (+10%) in the past relative to the present appear at odds with previous mass-balance calculations (Lécuyer et al. 1998, Parai & Mukhopadhyay 2012), continental freeboard studies (Galer 1991, Korenaga et al. 2017), and observations of constant ocean salinity over geological times (Marty et al. 2018), which indicate that the surface inventories of H_2O and Cl remained roughly constant through time (as also suggested by Kendrick et al. 2020). Our global mass balance indicates that ~70% of Cl is concentrated in Earth surface reservoirs [in line with previous estimates (Clay 2017)]. Our reconstruction of the past surface inventory of Cl, however, does not consider the fact that the fraction of surface Cl dissolved into the oceans versus stored onto continental platforms (e.g., in evaporite and brines) may not have been constant through time (Warren 2010). Below, we consider that the salinity of the oceans directly scales to the total inventory of surface Cl and investigate the implications of variable past recycling efficiencies of H_2O on the global evolution of the ocean budget and salinity.

As previously discussed, our calculations suggest that N influxes (constant over the past 2 Ga) may be decoupled from H_2O and Xe influxes [increasing over the past 1 Ga (Parai & Mukhopadhyay 2018)]. Here, the observation that our reconstruction of the past surface inventory of water (using the present-day mass balance) does not match geochemical and geodynamic constraints implies that at least one mechanism is missing from our approach and that we may be overestimating the efficiency of H_2O transport into the solid Earth by subduction. For instance, net subduction influxes considered in our model do not take into account outfluxes from the slab to the forearc/backarc, diffuse outgassing of H_2O at the arc, or the role of the continental crust as a volatile reservoir, which are likely important but largely unconstrained. Thermomechanical models of slab dehydration during subduction notably predict that up to ~25% (van Keken et al. 2018; see **Supplemental Text Section 1**) of water in the slab (sediments and AOC) may be lost to the forearc. Accounting for this additional loss of water from the slab results in a slightly lower net subduction flux, which decreases our modeled surface inventory of H_2O at 2 Ga and brings our estimate of past ocean salinity closer to the present-day value (**Figure 3*b***). However, this model would still require the total number of moles of H_2O at Earth's surface at 2 Ga to have been ~30% higher than that of today. Importantly, our result for H_2O is largely dependent on the assumed serpentinite flux, the global water outflux at arcs, and the extent of AOC alteration at the slab bend, which are not particularly well-constrained parameters. For example, if the present-day serpentinite flux was instead negligible, our mass balance would suggest a lower ingassing rate of H_2O (**Figure 2*c***), with an H_2O surface inventory at 2 Ga only about 10% higher than at present (instead of 50% higher when serpentinite is considered) (**Figure 3*b***), and hence a constant salinity over geological time. However, this possibility appears increasingly at odds with geophysical observations (Cai et al. 2018, Grevemeyer et al. 2018). We propose instead that this discrepancy may arise from the fact that, contrary to N, the recycling efficiency of H_2O changed through time. Steeper geotherms in the Precambrian (e.g., Ernst 2017), for example, may have limited the stability of serpentinite or other hydrous phases in the deep slab, whereas the subducting N budget is dominated by sediments and AOC. Variable rates of ocean plate production (e.g., Li et al. 2016) would also potentially impact the net ingassing rates of these two elements differently, as a larger proportion of N is for instance outgassed from oceanic ridges (**Table 2**).

Retaining a constant H_2O surface inventory through time would require lowering our estimate for the mean H_2O net ingassing flux at the arcs by ~80% (or alternatively increasing the mean H_2O outgassing flux from the DMM and PLM by a factor ~5), therefore producing a past salinity

Supplemental Material >

that is similar to salinity at present (Marty et al. 2018). Importantly, lowering our estimate for the Xe ingassing flux by the same amount would induce a negligible change in the surface Xe inventory. We therefore conclude that subduction influxes of different volatile elements (e.g., N versus H_2O and Xe) could have evolved differently over geological time, with lower net influxes of subducted H_2O and Xe in the past (Parai & Mukhopadhyay 2018) but roughly constant amounts of N (and potentially C and S) recycled through time. This difference is likely explained by biological oceanic N fixation that allows N in the form of ammonium (NH_4^+) to substitute for K in phyllosilicates such as mica, given that NH_4^+ and K share a similar charge and ionic radius (Busigny & Bebout 2013). Nitrogen can then be transported into the mantle, structurally bound within potassic minerals, with limited N loss, whereas the efficiency of H_2O, noble gas, and halogen transport into the mantle via hydrous mineral phases (e.g., serpentinites, amphiboles) may be more susceptible to loss due to higher ambient mantle temperatures in the past. In particular, phengite is known to be stable to depths of ~300 km and to be the dominate host phase for K (and many large-ion lithophile elements) recycling, making it a good candidate to also carry N into the mantle (Halama et al. 2010, Busigny & Bebout 2013). Other N-hosting mineral phases would then form at greater depth [e.g., phlogopite and amphiboles (Fumagalli et al. 2009); stishovite (Fukuyama et al. 2020)] and transport subducting N to the deep mantle. More research is required to identify the main carrier phases of major volatiles throughout the subduction process. For example, Li et al. (2019) recently argued that N and C isotope compositions of AOC may explain the range of N and C signatures observed in mantle diamonds, suggesting that AOC, instead of sediment, could represent the key carrier of crustal C and N into the deep mantle.

6. KNOWN UNKNOWNS AND FUTURE RESEARCH DIRECTIONS

In recent years, our understanding of subduction and volatile exchange between Earth's surface and interior has improved dramatically, and it is now accepted that volatile recycling has an overwhelming influence on the composition of Earth's interior. Improvements in data quality and mass-balance models allow an assessment of how and when volatile recycling commenced, and the potential effects this had on Earth dynamics. However, despite recent advances, many important open questions remain.

6.1. Hidden Reservoirs

We note that our model excludes several terrestrial reservoirs (e.g., the continental crust) that, although minor in scale, may be significant volatile repositories.

Due to its long-term stability, the SCLM may be a significant reservoir for subducted C, halogens, noble gases, and other volatiles (Kelemen & Manning 2015, Foley & Fischer 2017, Broadley et al. 2018). Direct analyses of fluids from the lithosphere trapped in diamonds and mantle xenoliths show that halogen concentrations can be several orders of magnitude greater than those measured in DMM- and PLM-derived samples (Broadley et al. 2018). However, the heterogeneous nature of the SCLM makes quantification of average volatile compositions for this reservoir challenging. It is clear that future analytical (diamond and xenolith), experimental, and modeling studies will be needed to investigate the role of the SCLM in sequestering subducted volatiles and relevant timescales.

The confidence in our understanding for each volatile reservoir inevitably decreases with increasing depth. Seismic imaging of the lower mantle shows significant thermochemical heterogeneity (Molnar 2019). While geochemical investigations provide evidence for the presence of

both recycled and primordial components that may explain these seismic observations, uncertainty remains with regard to the volume and volatile content of the lower mantle.

Natural ringwoodite inclusions in transition zone diamonds have been found to contain ~1 wt% H_2O (Pearson et al. 2014), suggesting the transition zone may contain as much as 2.5 surface ocean volumes of water (Nestola & Smyth 2016). Experiments have shown that F can be incorporated into transition zone minerals (wadsleyite and ringwoodite) in a similar manner to that for H_2O, indicating that the transition zone may constitute a significant reservoir for F, and likely also Cl, Br, and I (Roberge et al. 2015). The transition zone may act as a filter for other subducting volatiles; experiments suggest that carbonated oceanic crust may melt at transition zone depths, preventing C from being subducted deeper into the mantle (Thomson et al. 2016). However, data are limited, so further research is required.

Although their mineralogy is nominally anhydrous, olivine, pyroxene, and garnet can collectively carry greater than 0.4 wt% H_2O, and even greater concentrations are possible in lower mantle minerals (Hirschmann et al. 2005). The sheer size of the lower mantle makes it a significant reservoir for volatiles; however, how the volatile flux to the deep mantle evolved through time is dependent on many factors, including the timing of subduction initiation, time-integrated subduction efficiencies, the secular evolution of the geotherm, and the fate of oceanic material in the transition zone.

The core is perhaps the ultimate "known unknown," as it is unknown if it is a volatile source or a sink to the bulk silicate Earth. It is a significant reservoir of S, and potentially ^{3}He, C, and H (Bouhifd et al. 2013, Wu et al. 2018), but placing firm constraints on its volatile content is extremely challenging. As a result, the core's role in modulating the volatile content and isotopic compositions of Earth's mantle is largely unknown, but given its secular cooling, it is likely important (see **Supplemental Text Section 6.5** for more details).

Supplemental Material >

6.2. Hidden Fluxes

In order to construct a mass-balance model, we compiled outfluxes from MORs, mantle plumes, and volcanic arcs, which represent the main sources of volcanic outgassing. However, outgassing rates have inherent uncertainties, and several potential sources are not considered in our calculations.

Volatile outfluxes are relatively well constrained from direct degassing measurements at volcanic sites; however, diffuse release of volatiles is often overlooked. For example, diffuse tectonic C degassing rates in continental rift settings have been estimated to be equivalent to total MOR fluxes (Lee et al. 2016), and significant diffuse outgassing of CO_2 has also been detected in global forearcs (Campbell et al. 2002, Fryer 2012). Here, preliminary considerations on the extent of diffuse CO_2 emissions (Fischer et al. 2019) have been considered for the C mass balance (**Figure 3*a***), but the extent of diffuse degassing of other volatiles—which could also be significant—remains unknown. Further improving our understanding of global volatile outfluxes will require better quantification of the contributions from weak emitters, diffuse degassing, explosive volcanism, and background biogenic sources (Fischer et al. 2019), as well as sequestering processes (e.g., calcite formation) in the forearc region (Barry et al. 2019).

The subduction of volatiles to the core–mantle boundary (CMB) could result in bidirectional volatile fluxes at that critical interface. If volatiles are subducted to the CMB, fluids may react with the underlying iron, forming iron hydrides (FeH_x) and hydrates (FeO_2H_x), which could potentially explain the seismic ultralow velocity zone at the base of the mantle (Mao et al. 2017). Furthermore, the progressive dissolution of H into the core, and the strong interactions between H and other solutes in liquid Fe, may result in the expulsion of minor element components back into the mantle.

SUMMARY POINTS

1. We compute volatile concentrations and fluxes using published data and present them within the context of an internally mass-balanced model of volatile recycling.
2. At subduction zones, all volatiles (apart from He and Ne) are transported past the arc and into the mantle (i.e., recycling efficiencies greater than 0%).
3. When influxes (subduction) are balanced with total outfluxes (volcanism), N, H_2O, C, and most likely heavy noble gases are shown to be in a net global ingassing state.
4. We present an isotopically constrained N box model that suggests that subduction of N began ca. 2 Ga and N subduction influxes remained roughly constant until today.
5. Extrapolating the modern ingassing/outgassing state over the past 2 Gyr produces satisfactory results for all volatile elements apart from H_2O, suggesting that it is decoupled from N, perhaps due to their fundamentally different transport mechanisms during subduction (chemical fixation in sediments versus physical trapping in pore fluids).

FUTURE ISSUES

1. What was the volatile isotopic and abundance composition of the initial mantle prior to subduction?
2. What are the respective roles of accretion/core formation processes in setting the initial volatile inventory of the mantle?
3. How does the integrated history of volatile recycling account for the present-day complexity of the mantle zoo (e.g., enriched mantle 1, enriched mantle 2, FOcus ZOne, and high μ mantle domain end members)?
4. What are the mechanisms that control recycling efficiency of volatile elements through time (e.g., secular cooling of the mantle, plate tectonics, subduction mechanisms)?
5. What is the contribution of diffuse degassing/forearc loss to the global outflux of volatiles?
6. What is the role of the continental crust in modulating Earth's volatile cycles?
7. Can multiple isotope systematics (e.g., Xe, N, H, Cl) be combined to better constrain past volatile recycling efficiency?
8. What are the implications of episodic geological events (e.g., emplacement of large igneous provinces) on the global volatile mass balance?

DISCLOSURE STATEMENT

The authors are not aware of any affiliations, memberships, funding, or financial holdings that might be perceived as affecting the objectivity of this review.

ACKNOWLEDGMENTS

We are extremely grateful to reviewers Terry Plank, Bernard Marty, Mark Kendrick, Tobias Fischer, Long Li, and Andy Smye for their constructive insights. We also thank Production Editor

Annie Beck and an anonymous *AR Earth and Planetary Sciences* Editorial Committee Member for helpful comments. This work was supported by NSF award 2015789 to P.H.B.

LITERATURE CITED

Ader M, Thomazo C, Sansjofre P, Busigny V, Papineau D, et al. 2016. Interpretation of the nitrogen isotopic composition of Precambrian sedimentary rocks: assumptions and perspectives. *Chem. Geol.* 429:93–110

Ague JJ, Nicolescu S. 2014. Carbon dioxide released from subduction zones by fluid-mediated reactions. *Nat. Geosci.* 7(5):355–60

Aiuppa A, Fischer TP, Plank T, Robidoux P, Di Napoli R. 2017. Along-arc, inter-arc and arc-to-arc variations in volcanic gas CO_2/S_T ratios reveal dual source of carbon in arc volcanism. *Earth-Sci. Rev.* 168:24–47

Alexander COD, Bowden R, Fogel ML, Howard KT, Herd CDK, Nittler LR. 2012. The provenances of asteroids, and their contributions to the volatile inventories of the terrestrial planets. *Science* 337(6095):721–23

Allègre CJ. 1982. Chemical geodynamics. *Tectonophysics* 81(3–4):109–32

Allègre CJ, Hofmann A, O'Nions K. 1996. The argon constraints on mantle structure. *Geophys. Res. Lett.* 23(24):3555–57

Alt JC. 1995. Sulfur isotopic profile through the oceanic crust: sulfur mobility and seawater-crustal sulfur exchange during hydrothermal alteration. *Geology* 23(7):585–88

Alt JC. 2003. Stable isotopic composition of upper oceanic crust formed at a fast spreading ridge, ODP Site 801. *Geochem. Geophys. Geosyst.* 4:8908

Alt JC, Garrido CJ, Shanks WC III, Turchyn A, Padrón-Navarta JA, et al. 2012. Recycling of water, carbon, and sulfur during subduction of serpentinites: a stable isotope study of Cerro del Almirez, Spain. *Earth Planet. Sci. Lett.* 327:50–60

Alt JC, Shanks WC. 2011. Microbial sulfate reduction and the sulfur budget for a complete section of altered oceanic basalts, IODP Hole 1256D (eastern Pacific). *Earth Planet. Sci. Lett.* 310(1–2):73–83

Arevalo R Jr., McDonough WF, Luong M. 2009. The K/U ratio of the silicate Earth: insights into mantle composition, structure and thermal evolution. *Earth Planet. Sci. Lett.* 278(3–4):361–69

Avice G, Marty B, Burgess R, Hofmann A, Philippot P, et al. 2018. Evolution of atmospheric xenon and other noble gases inferred from Archean to Paleoproterozoic rocks. *Geochim. Cosmochim. Acta* 232:82–100

Barnes JD, Cisneros M. 2012. Mineralogical control on the chlorine isotope composition of altered oceanic crust. *Chem. Geol.* 326:51–60

Barnes JD, Manning CE, Scambelluri M, Selverstone J. 2018. The behavior of halogens during subduction-zone processes. In *The Role of Halogens in Terrestrial and Extraterrestrial Geochemical Processes*, ed. DE Harlov, L Aranovich, pp. 545–90. Cham, Switz.: Springer

Barnes JD, Sharp ZD. 2006. A chlorine isotope study of DSDP/ODP serpentinized ultramafic rocks: insights into the serpentinization process. *Chem. Geol.* 228(4):246–65

Barnes JD, Sharp ZD, Fischer TP. 2008. Chlorine isotope variations across the Izu-Bonin-Mariana arc. *Geology* 36(11):883–86

Barnes JD, Sharp ZD, Fischer TP, Hilton DR, Carr MJ. 2009. Chlorine isotope variations along the Central American volcanic front and back arc. *Geochem. Geophys. Geosyst.* 10(11):Q11S17

Barnes JD, Straub SM. 2010. Chorine stable isotope variations in Izu Bonin tephra: implications for serpentinite subduction. *Chem. Geol.* 272(1–4):62–74

Barry PH, de Moor JM, Giovannelli D, Schrenk M, Hummer DR, et al. 2019. Forearc carbon sink reduces long-term volatile recycling into the mantle. *Nature* 568(7753):487–92

Barry PH, Hilton DR. 2016. Release of subducted sedimentary nitrogen throughout Earth's mantle. *Geochem. Perspect. Lett.* 2:148–59

Barry PH, Hilton DR, Füri E, Halldórsson SA, Grönvold K. 2014. Carbon-isotope and abundance systematics of Icelandic geothermal gases, fluids and subglacial basalts with implications for mantle plume-related CO_2 fluxes. *Geochim. Cosmochim. Acta* 134:74–99

Behn MD, Kelemen PB, Hirth G, Hacker BR, Massonne HJ. 2011. Diapirs as the source of the sediment signature in arc lavas. *Nat. Geosci.* 4(9):641–46

Bekaert DV, Broadley MW, Caracausi A, Marty B. 2019. Novel insights into the degassing history of Earth's mantle from high precision noble gas analysis of magmatic gas. *Earth Planet. Sci. Lett.* 525:115766

Demonstrates the importance of forearc calcite precipitation and microbial uptake for the C recycling mass balance.

Presents a N subduction model that explains the evolution of the mantle's N-isotope composition.

Bergin EA, Blake GA, Ciesla F, Hirschmann MM, Li J. 2015. Tracing the ingredients for a habitable earth from interstellar space through planet formation. *PNAS* 112(29):8965–70

Berner RA, Raiswell R. 1984. C/S method for distinguishing freshwater from marine sedimentary rocks. *Geology* 12(6):365–68

Bernini D, Wiedenbeck M, Dolejš D, Keppler H. 2013. Partitioning of halogens between mantle minerals and aqueous fluids: implications for the fluid flow regime in subduction zones. *Contrib. Mineral. Petrol.* 165(1):117–28

Beyer C, Klemme S, Wiedenbeck M, Stracke A, Vollmer C. 2012. Fluorine in nominally fluorine-free mantle minerals: experimental partitioning of F between olivine, orthopyroxene and silicate melts with implications for magmatic processes. *Earth Planet. Sci. Lett.* 337:1–9

Reports global MOR and arc lengths that prominently feed into the model presented here.

Bird P. 2003. An updated digital model of plate boundaries. *Geochem. Geophys. Geosyst.* 4(3):1027

Bouhifd MA, Jephcoat AP, Heber VS, Kelley SP. 2013. Helium in Earth's early core. *Nat. Geosci.* 6(11):982–86

Broadley MW, Ballentine CJ, Chavrit D, Dallai L, Burgess R. 2016. Sedimentary halogens and noble gases within Western Antarctic xenoliths: implications of extensive volatile recycling to the sub continental lithospheric mantle. *Geochim. Cosmochim. Acta* 176:139–56

Broadley MW, Barry PH, Ballentine CJ, Taylor LA, Burgess R. 2018. End-Permian extinction amplified by plume-induced release of recycled lithospheric volatiles. *Nat. Geosci.* 11(9):682–87

Broadley MW, Barry PH, Bekaert DV, Byrne DJ, Caracausi A, et al. 2020. Identification of chondritic krypton and xenon in Yellowstone gases and the timing of terrestrial volatile accretion. *PNAS* 117:13997–14004

Brown M. 2006. Duality of thermal regimes is the distinctive characteristic of plate tectonics since the Neoarchean. *Geology* 34(11):961–64

Busigny V, Bebout GE. 2013. Nitrogen in the silicate Earth: speciation and isotopic behavior during mineral–fluid interactions. *Elements* 9(5):353–58

Busigny V, Cartigny P, Laverne C, Teagle D, Bonifacie M, Agrinier P. 2019. A re-assessment of the nitrogen geochemical behavior in upper oceanic crust from Hole 504B: implications for subduction budget in Central America. *Earth Planet. Sci. Lett.* 525:115735

Busigny V, Cartigny P, Philippot P. 2011. Nitrogen-isotopes in ophiolitic metagabbros: a re-evaluation of modern nitrogen fluxes in subduction zones and implication for the early Earth atmosphere. *Geochim. Cosmochim. Acta* 75(23):7502–21

Busigny V, Cartigny P, Philippot P, Ader M, Javoy M. 2003. Massive recycling of nitrogen and other fluid-mobile elements (K, Rb, Cs, H) in a cold slab environment: evidence from HP to UHP oceanic metasediments of the Schistes Lustrés nappe (western Alps, Europe). *Earth Planet. Sci. Lett.* 215(1–2):27–42

Cabral RA, Jackson MG, Rose-Koga EF, Koga KT, Whitehouse MJ, et al. 2013. Anomalous sulphur isotopes in plume lavas reveal deep mantle storage of Archaean crust. *Nature* 496(7446):490–93

Cai C, Wiens DA, Shen W, Eimer M. 2018. Water input into the Mariana subduction zone estimated from ocean-bottom seismic data. *Nature* 563(7731):389–92

Campbell KA, Farmer JD, Des Marais D. 2002. Ancient hydrocarbon seeps from the Mesozoic convergent margin of California: carbonate geochemistry, fluids and palaeoenvironments. *Geofluids* 2(2):63–94

Carlson RL, Miller DJ. 2003. Mantle wedge water contents estimated from seismic velocities in partially serpentinized peridotites. *Geophys. Res. Lett.* 30(5):1250

Carn SA, Fioletov VE, McLinden CA, Li C, Krotkov NA. 2017. A decade of global volcanic SO_2 emissions measured from space. *Sci. Rep.* 7:44095

Cartigny P, Marty B. 2013. Nitrogen isotopes and mantle geodynamics: the emergence of life and the atmosphere–crust–mantle connection. *Elements* 9(5):359–66

Cartigny P, Palot M, Thomassot E, Harris JW. 2014. Diamond formation: a stable isotope perspective. *Annu. Rev. Earth Planet. Sci.* 42:699–732

Cartigny P, Pineau F, Aubaud C, Javoy M. 2008. Towards a consistent mantle carbon flux estimate: insights from volatile systematics (H_2O/Ce, δD, CO_2/Nb) in the North Atlantic mantle (14°N and 34°N). *Earth Planet. Sci. Lett.* 265(3–4):672–85

Chaussidon M, Albarède F, Sheppard SM. 1989. Sulphur isotope variations in the mantle from ion microprobe analyses of micro-sulphide inclusions. *Earth Planet. Sci. Lett.* 92(2):144–56

Chavrit D, Burgess R, Sumino H, Teagle DA, Droop G, et al. 2016. The contribution of hydrothermally altered ocean crust to the mantle halogen and noble gas cycles. *Geochim. Cosmochim. Acta* 183:106–24

Clay PL, Burgess R, Busemann H, Ruzié-Hamilton L, Joachim B, et al. 2017. Halogens in chondritic meteorites and terrestrial accretion. *Nature* 551(7682):614–18

Clift PD. 2017. A revised budget for Cenozoic sedimentary carbon subduction. *Rev. Geophys.* 55(1):97–125

Clog M, Aubaud C, Cartigny P, Dosso L. 2013. The hydrogen isotopic composition and water content of southern Pacific MORB: a reassessment of the D/H ratio of the depleted mantle reservoir. *Earth Planet. Sci. Lett.* 381:156–65

Cottaar S, Lekic V. 2016. Morphology of seismically slow lower-mantle structures. *Geophys. J. Int.* 207(2):1122–36

Crisp JA. 1984. Rates of magma emplacement and volcanic output. *J. Volcanol. Geotherm. Res.* 20:177–211

Dalou C, Füri E, Deligny C, Piani L, Caumon MC, et al. 2019. Redox control on nitrogen isotope fractionation during planetary core formation. *PNAS* 116(29):14485–94

Dalou C, Koga KT, Shimizu N, Boulon J, Devidal JL. 2012. Experimental determination of F and Cl partitioning between lherzolite and basaltic melt. *Contrib. Mineral. Petrol.* 163(4):591–609

Dasgupta R, Hirschmann MM. 2010. The deep carbon cycle and melting in Earth's interior. *Earth Planet. Sci. Lett.* 298(1–2):1–13

Dauphas N. 2017. The isotopic nature of the Earth's accreting material through time. *Nature* 541(7638):521–24

Dixon JE, Clague DA. 2001. Volatiles in basaltic glasses from Loihi Seamount, Hawaii: evidence for a relatively dry plume component. *J. Petrol.* 42(3):627–54

Dixon JE, Leist L, Langmuir C, Schilling JG. 2002. Recycled dehydrated lithosphere observed in plume-influenced mid-ocean-ridge basalt. *Nature* 420(6914):385–89

Dottin JW III, Labidi J, Jackson MG, Woodhead JD, Farquhar J. 2020a. Isotopic evidence for multiple recycled sulfur reservoirs in the Mangaia mantle plume. *Geochem. Geophys. Geosyst.* 21(10):e2020GC009081

Dottin JW III, Labidi J, Lekic V, Jackson MG, Farquhar J. 2020b. Sulfur isotope characterization of primordial and recycled sources feeding the Samoan mantle plume. *Earth Planet. Sci. Lett.* 534:116073

Ducea MN, Paterson SR, DeCelles PG. 2015. High-volume magmatic events in subduction systems. *Elements* 11(2):99–104

Duncan MS, Dasgupta R. 2017. Rise of Earth's atmospheric oxygen controlled by efficient subduction of organic carbon. *Nat. Geosci.* 10(5):387–92

Ernst WG. 2017. Earth's thermal evolution, mantle convection, and Hadean onset of plate tectonics. *J. Asian Earth Sci.* 145:334–48

Fabbrizio A, Stalder R, Hametner K, Günther D, Marquardt K. 2013. Experimental partitioning of halogens and other trace elements between olivine, pyroxenes, amphibole and aqueous fluid at 2 GPa and 900–1,300°C. *Contrib. Mineral. Petrol.* 166(2):639–53

Faccenda M, Gerya TV, Mancktelow NS, Moresi L. 2012. Fluid flow during slab unbending and dehydration: implications for intermediate-depth seismicity, slab weakening and deep water recycling. *Geochem. Geophys. Geosyst.* 13(1):Q01010

Fischer TP. 2008. Fluxes of volatiles (H_2O, CO_2, N_2, Cl, F) from arc-volcanoes. *Geochem. J.* 42(1):21–38

Fischer TP, Arellano S, Carn S, Aiuppa A, Galle B, et al. 2019. The emissions of CO_2 and other volatiles from the world's subaerial volcanoes. *Sci. Rep.* 9(1):18716

Presents an updated assessment of CO_2 and SO_2 outflux estimates and their related caveats.

Fischer TP, Aiuppa A. 2020. AGU centennial grand challenge: volcanoes and deep carbon global CO_2 emissions from subaerial volcanism—recent progress and future challenges. *Geochem. Geophys. Geosyst.* 21(3):e2019GC008690

Fischer TP, Marty B. 2005. Volatile abundances in the sub-arc mantle: insights from volcanic and hydrothermal gas discharges. *J. Volcanol. Geotherm. Res.* 140(1–3):205–16

Foley SF, Fischer TP. 2017. An essential role for continental rifts and lithosphere in the deep carbon cycle. *Nat. Geosci.* 10(12):897–902

Fryer P. 2012. Serpentinite mud volcanism: observations, processes, and implications. *Annu. Rev. Mar. Sci.* 4:345–73

Fukuyama K, Kagi H, Inoue T, Kakizawa S, Shinmei T, et al. 2020. High nitrogen solubility in stishovite (SiO_2) under lower mantle conditions. *Sci. Rep.* 10(1):10897

Fumagalli P, Zanchetta S, Poli S. 2009. Alkali in phlogopite and amphibole and their effects on phase relations in metasomatized peridotites: a high-pressure study. *Contrib. Mineral. Petrol.* 158(6):723

Galer SJG. 1991. Interrelationships between continental freeboard, tectonics and mantle temperature. *Earth Planet. Sci. Lett.* 105(1–3):214–28

Galle B, Oppenheimer CM, Geyer A, McGonigle A, Edmonds M. 2003. A mini-DOAS spectrometer applied in remote sensing of volcanic SO_2 emissions. *J. Volcanol. Geotherm. Res.* 119(1–4):241–54

Gavrilenko M, Krawczynski M, Ruprecht P, Li W, Catalano JG. 2019. The quench control of water estimates in convergent margin magmas. *Am. Mineral.* 104(7):936–48

Goldschmidt VM. 1954. *Geochemistry*. Oxford, UK: Clarendon

Gonnermann HM, Mukhopadhyay S. 2007. Non-equilibrium degassing and a primordial source for helium in ocean-island volcanism. *Nature* 449(7165):1037–40

Gonnermann HM, Mukhopadhyay S. 2009. Preserving noble gases in a convecting mantle. *Nature* 459(7246):560–63

Gorman PJ, Kerrick DM, Connolly JAD. 2006. Modeling open system metamorphic decarbonation of subducting slabs. *Geochem. Geophys. Geosyst.* 7(4):Q04007

Grevemeyer I, Ranero CR, Ivandic M. 2018. Structure of oceanic crust and serpentinization at subduction trenches. *Geosphere* 14(2):395–418

Grove TL, Till CB. 2019. H_2O-rich mantle melting near the slab–wedge interface. *Contrib. Mineral. Petrol.* 174(10):80

Hacker BR. 2008. H_2O subduction beyond arcs. *Geochem. Geophys. Geosyst.* 9(3):Q03001

Halama R, Bebout GE, John T, Scambelluri M. 2014. Nitrogen recycling in subducted mantle rocks and implications for the global nitrogen cycle. *Int. J. Earth Sci.* 103(7):2081–99

Halama R, Bebout GE, John T, Schenk V. 2010. Nitrogen recycling in subducted oceanic lithosphere: the record in high- and ultrahigh-pressure metabasaltic rocks. *Geochim. Cosmochim. Acta* 74(5):1636–52

Hallis LJ, Huss GR, Nagashima K, Taylor GJ, Halldórsson SA, et al. 2015. Evidence for primordial water in Earth's deep mantle. *Science* 350(6262):795–97

Hilton DR, Fischer TP, Marty B. 2002. Noble gases and volatile recycling at subduction zones. *Rev. Mineral. Geochem.* 47(1):319–70

Hilton DR, Thirlwall MF, Taylor RN, Murton BJ, Nichols A. 2000. Controls on magmatic degassing along the Reykjanes Ridge with implications for the helium paradox. *Earth Planet. Sci. Lett.* 183(1–2):43–50

Hirschmann MM. 2018. Comparative deep Earth volatile cycles: the case for C recycling from exosphere/mantle fractionation of major (H_2O, C, N) volatiles and from H_2O/Ce, CO_2/Ba, and CO_2/Nb exosphere ratios. *Earth Planet. Sci. Lett.* 502:262–73

Hirschmann MM, Aubaud C, Withers AC. 2005. Storage capacity of H_2O in nominally anhydrous minerals in the upper mantle. *Earth Planet. Sci. Lett.* 236(1–2):167–81

Hirschmann MM, Dasgupta R. 2009. The H/C ratios of Earth's near-surface and deep reservoirs, and consequences for deep Earth volatile cycles. *Chem. Geol.* 262(1–2):4–16

Holder RM, Viete DR, Brown M, Johnson TE. 2019. Metamorphism and the evolution of plate tectonics. *Nature* 572(7769):378–81

Presents evidence for the ubiquity of recycled volatiles in the mantle, using heavy noble gases.

Holland G, Ballentine CJ. 2006. Seawater subduction controls the heavy noble gas composition of the mantle. *Nature* 441(7090):186–91

Holland G, Ballentine CJ, Cassidy M. 2009. Primordial krypton in the terrestrial mantle is not solar. *LPI* 2009:1824

Holloway JR, Jakobsson S. 1986. Volatile solubilities in magmas: transport of volatiles from mantles to planet surfaces. *J. Geophys. Res.* 91(B4):505–8

Holzer M, DeVries T, Bianchi D, Newton R, Schlosser P, Winckler G. 2017. Objective estimates of mantle ^{3}He in the ocean and implications for constraining the deep ocean circulation. *Earth Planet. Sci. Lett.* 458:305–14

Hopkins M, Harrison TM, Manning CE. 2008. Low heat flow inferred from >4 Gyr zircons suggests Hadean plate boundary interactions. *Nature* 456(7221):493–96

Jackson MG, Jellinek AM. 2013. Major and trace element composition of the high ^{3}He/^{4}He mantle: implications for the composition of a nonchonditic Earth. *Geochem. Geophys. Geosyst.* 14(8):2954–76

Jambon A. 1994. Earth degassing and large-scale geochemical cycling of volatile elements. *Rev. Mineral. Geochem.* 30(1):479–517

Jarrard RD. 2003. Subduction fluxes of water, carbon dioxide, chlorine, and potassium. *Geochem. Geophys. Geosyst.* 4(5):8905

Javaux EJ. 2019. Challenges in evidencing the earliest traces of life. *Nature* 572(7770):451–60

Javoy M, Kaminski E, Guyot F, Andrault D, Sanloup C, et al. 2010. The chemical composition of the Earth: enstatite chondrite models. *Earth Planet. Sci. Lett.* 293(3–4):259–68

Javoy M, Pineau F. 1991. The volatiles record of a "popping" rock from the Mid-Atlantic Ridge at 14°N: chemical and isotopic composition of gas trapped in the vesicles. *Earth Planet. Sci. Lett.* 107(3–4):598–611

Jicha BR, Jagoutz O. 2015. Magma-production rates for intraoceanic arcs. *Elements* 11(2):105–11

John T, Layne GD, Haase KM, Barnes JD. 2010. Chlorine isotope evidence for crustal recycling into the Earth's mantle. *Earth Planet. Sci. Lett.* 298(1–2):175–82

John T, Scambelluri M, Frische M, Barnes JD, Bach W. 2011. Dehydration of subducting serpentinite: implications for halogen mobility in subduction zones and the deep halogen cycle. *Earth Planet. Sci. Lett.* 308(1–2):65–76

Johnson HP, Semyan SW. 1994. Age variation in the physical properties of oceanic basalts: implications for crustal formation and evolution. *J. Geophys. Res.* 99(B2):3123–34

Kagoshima T, Sano Y, Takahata N, Maruoka T, Fischer TP, Hattori K. 2015. Sulphur geodynamic cycle. *Sci. Rep.* 5(1):8330

Kalacheva EG, Taran YA, Voloshina EV, Kotenko TA. 2018. Geochemistry of thermal waters of Ketoi Island, Kuril Island arc. *J. Volcanol. Seismol.* 12(3):172–86

Kelemen PB, Manning CE. 2015. Reevaluating carbon fluxes in subduction zones, what goes down, mostly comes up. *PNAS* 112(30):E3997–4006

Keller B, Schoene B. 2018. Plate tectonics and continental basaltic geochemistry throughout Earth history. *Earth Planet. Sci. Lett.* 481:290–304

Kendrick MA. 2019a. Halogens in altered ocean crust from the East Pacific Rise (ODP/IODP Hole 1256D). *Geochim. Cosmochim. Acta* 261:93–112

Kendrick MA. 2019b. Halogens in Atlantis Bank gabbros, SW Indian Ridge: implications for styles of seafloor alteration. *Earth Planet. Sci. Lett.* 514:96–107

Kendrick MA, Danyushevsky LV, Falloon TJ, Woodhead JD, Arculus RJ, Ireland T. 2020. SW Pacific arc and backarc lavas and the role of slab-bend serpentinites in the global halogen cycle. *Earth Planet. Sci. Lett.* 530:115921

Kendrick MA, Hémond C, Kamenetsky VS, Danyushevsky L, Devey CW, et al. 2017. Seawater cycled throughout Earth's mantle in partially serpentinized lithosphere. *Nat. Geosci.* 10(3):222–28

Kendrick MA, Honda M, Oliver NHS, Phillips D. 2011. The noble gas systematics of late-orogenic H_2O–CO_2 fluids, Mt Isa, Australia. *Geochim. Cosmochim. Acta* 75(6):1428–50

Kendrick MA, Honda M, Pettke T, Scambelluri M, Phillips D, Giuliani A. 2013. Subduction zone fluxes of halogens and noble gases in seafloor and forearc serpentinites. *Earth Planet. Sci. Lett.* 365:86–96

Kendrick MA, Jackson MG, Hauri EH, Phillips D. 2015. The halogen (F, Cl, Br, I) and H_2O systematics of Samoan lavas: assimilated-seawater, EM2 and high-$^3He/^4He$ components. *Earth Planet. Sci. Lett.* 410:197–209

Kendrick MA, Jackson MG, Kent AJ, Hauri EH, Wallace PJ, Woodhead J. 2014. Contrasting behaviours of CO_2, S, H_2O and halogens (F, Cl, Br, and I) in enriched-mantle melts from Pitcairn and Society seamounts. *Chem. Geol.* 370:69–81

Kendrick MA, Scambelluri M, Hermann J, Padrón-Navarta JA. 2018. Halogens and noble gases in serpentinites and secondary peridotites: implications for seawater subduction and the origin of mantle neon. *Geochim. Cosmochim. Acta* 235:285–304

Kerrick DM, Connolly JAD. 2001. Metamorphic devolatilization of subducted marine sediments and the transport of volatiles into the Earth's mantle. *Nature* 411(6835):293–96

Kobayashi M, Sumino H, Nagao K, Ishimaru S, Arai S, et al. 2017. Slab-derived halogens and noble gases illuminate closed system processes controlling volatile element transport into the mantle wedge. *Earth Planet. Sci. Lett.* 457:106–16

Korenaga J. 2013. Initiation and evolution of plate tectonics on Earth: theories and observations. *Annu. Rev. Earth Planet. Sci.* 41:117–51

Korenaga J, Planavsky NJ, Evans DA. 2017. Global water cycle and the coevolution of the Earth's interior and surface environment. *Philos. Trans. R. Soc. A* 375:20150393

Krawczynski M, Grove TL. 2019. The super-hydrous component of the Mt. Shasta plumbing system. *AGUFM* 2019:T23G-0512

Shows that non-atmospheric, isotopically heavy N occurs in plume-derived samples, using clumped N isotopes.

Labidi J, Barry PH, Bekaert DV, Broadley MW, Marty B, et al. 2020. Hydrothermal $^{15}N^{15}N$ abundances constrain the origins of mantle nitrogen. *Nature* 580(7803):367–71

Labidi J, Cartigny P. 2016. Negligible sulfur isotope fractionation during partial melting: evidence from Garrett transform fault basalts, implications for the late-veneer and the hadean matte. *Earth Planet. Sci. Lett.* 451:196–207

Labidi J, Cartigny P, Jackson MG. 2015. Multiple sulfur isotope composition of oxidized Samoan melts and the implications of a sulfur isotope 'mantle array' in chemical geodynamics. *Earth Planet. Sci. Lett.* 417:28–39

Labidi J, Cartigny P, Moreira M. 2013. Non-chondritic sulphur isotope composition of the terrestrial mantle. *Nature* 501(7466):208–11

le Roux PJ, Shirey SB, Hauri EH, Perfit MR, Bender JF. 2006. The effects of variable sources, processes and contaminants on the composition of northern EPR MORB (8–10°N and 12–14°N): evidence from volatiles (H_2O, CO_2, S) and halogens (F, Cl). *Earth Planet. Sci. Lett.* 251(3–4):209–31

Le Voyer M, Hauri EH, Cottrell E, Kelley KA, Salters VJ, et al. 2019. Carbon fluxes and primary magma CO_2 contents along the global mid-ocean ridge system. *Geochem. Geophys. Geosyst.* 20(3):1387–424

Le Voyer M, Kelley KA, Cottrell E, Hauri EH. 2017. Heterogeneity in mantle carbon content from CO_2-undersaturated basalts. *Nat. Commun.* 8(1):14062

Lécuyer C, Gillet P, Robert F. 1998. The hydrogen-isotope composition of seawater and the global water cycle. *Chem. Geol.* 145(3–4):249–61

Lee H, Muirhead JD, Fischer TP, Ebinger CJ, Kattenhorn SA, et al. 2016. Massive and prolonged deep carbon emissions associated with continental rifting. *Nat. Geosci.* 9(2):145–49

Li K, Li L, Pearson DG, Stachel T. 2019. Diamond isotope compositions indicate altered igneous oceanic crust dominates deep carbon recycling. *Earth Planet. Sci. Lett.* 516:190–201

Li L, Bebout GE. 2005. Carbon and nitrogen geochemistry of sediments in the Central American convergent margin: insights regarding subduction input fluxes, diagenesis, and paleoproductivity. *J. Geophys. Res.* 110(B11):B11202

Li L, Bebout GE, Idleman BD. 2007. Nitrogen concentration and $\delta^{15}N$ of altered oceanic crust obtained on ODP Legs 129 and 185: insights into alteration-related nitrogen enrichment and the nitrogen subduction budget. *Geochim. Cosmochim. Acta* 71(9):2344–60

Li L, Zheng Y-F, Cartigny C, Li J. 2014. Anomalous nitrogen isotopes in ultrahigh-pressure metamorphic rocks from the Sulu orogenic belt: effect of abiotic nitrogen reduction during fluid–rock interaction. *Earth Planetary Sci. Lett.* 403:67–78

Li M, Black B, Zhong S, Manga M, Rudolph ML, Olson P. 2016. Quantifying melt production and degassing rate at mid-ocean ridges from global mantle convection models with plate motion history. *Geochem. Geophys. Geosyst.* 17(7):2884–904

Loewen MW, Graham DW, Bindeman IN, Lupton JE, Garcia MO. 2019. Hydrogen isotopes in high $^3He/^4He$ submarine basalts: primordial versus recycled water and the veil of mantle enrichment. *Earth Planet. Sci. Lett.* 508:62–73

Lorand JP, Luguet A. 2016. Chalcophile and siderophile elements in mantle rocks: trace elements controlled by trace minerals. *Rev. Mineral. Geochem.* 81(1):441–88

Mao HK, Hu Q, Yang L, Liu J, Kim DY, et al. 2017. When water meets iron at Earth's core–mantle boundary. *Natl. Sci. Rev.* 4(6):870–78

Introduced the notion that Earth's mantle evolved due to subduction of isotopically heavy sedimentary N.

Marty B. 2012. The origins and concentrations of water, carbon, nitrogen and noble gases on Earth. *Earth Planet. Sci. Lett.* 313:56–66

Marty B, Avice G, Bekaert DV, Broadley MW. 2018. Salinity of the Archaean oceans from analysis of fluid inclusions in quartz. *C. R. Geosci.* 350(4):154–63

Marty B, Dauphas N. 2003. The nitrogen record of crust–mantle interaction and mantle convection from Archean to present. *Earth Planet. Sci. Lett.* 206(3–4):397–410

Marty B, Tolstikhin IN. 1998. CO_2 fluxes from mid-ocean ridges, arcs and plumes. *Chem. Geol.* 145(3–4):233–48

Marty B, Zimmermann L. 1999. Volatiles (He, C, N, Ar) in mid-ocean ridge basalts: assesment of shallow-level fractionation and characterization of source composition. *Geochim. Cosmochim. Acta* 63(21):3619–33

Marty B, Zimmermann L, Pujol M, Burgess R, Philippot P. 2013. Nitrogen isotopic composition and density of the Archean atmosphere. *Science* 342(6154):101–4

Matsuda JI, Nagao K. 1986. Noble gas abundances in a deep-sea sediment core from eastern equatorial Pacific. *Geochem. J.* 20(2):71–80

Matsumoto T, Pinti DL, Matsuda JI, Umino S. 2002. Recycled noble gas and nitrogen in the subcontinental lithospheric mantle: implications from N-He-Ar in fluid inclusions of SE Australian xenoliths. *Geochem. J.* 36(3):209–17

Mattey DP, Carr RH, Wright IP, Pillinger CT. 1984. Carbon isotopes in submarine basalts. *Earth Planet. Sci. Lett.* 70(2):196–206

McCaig AM, Titarenko SS, Savov IP, Cliff RA, Banks D, et al. 2018. No significant boron in the hydrated mantle of most subducting slabs. *Nat. Commun.* 9(1):4602

McGovern PJ, Schubert G. 1989. Thermal evolution of the Earth: effects of volatile exchange between atmosphere and interior. *Earth Planet. Sci. Lett.* 96(1–2):27–37

Michael PJ, Graham DW. 2015. The behavior and concentration of CO_2 in the suboceanic mantle: inferences from undegassed ocean ridge and ocean island basalts. *Lithos* 236:338–51

Mikhail S, Sverjensky DA. 2014. Nitrogen speciation in upper-mantle fluids and the origin of Earth's nitrogen-rich atmosphere. *Nat. Geosci.* 7(11):816–19

Miller WG, Maclennan J, Shorttle O, Gaetani GA, Le Roux V, Klein F. 2019. Estimating the carbon content of the deep mantle with Icelandic melt inclusions. *Earth Planet. Sci. Lett.* 523:115699

Mitchell EC, Fischer TP, Hilton DR, Hauri EH, Shaw AM, et al. 2010. Nitrogen sources and recycling at subduction zones: insights from the Izu-Bonin-Mariana arc. *Geochem. Geophys. Geosyst.* 11(2):Q02X11

Molnar P. 2019. Lower mantle dynamics perceived with 50 years of hindsight from plate tectonics. *Geochem. Geophys. Geosyst.* 20(12):5619–49

Moore LR, Gazel E, Tuohy R, Lloyd AS, Esposito R, et al. 2015. Bubbles matter: an assessment of the contribution of vapor bubbles to melt inclusion volatile budgets. *Am. Mineral.* 100(4):806–23

Moreira M, Kunz J, Allègre C. 1998. Rare gas systematics in popping rock: isotopic and elemental compositions in the upper mantle. *Science* 279(5354):1178–81

Mori T, Shinohara H, Kazahaya K, Hirabayashi JI, Matsushima T, et al. 2013. Time-averaged SO_2 fluxes of subduction-zone volcanoes: example of a 32-year exhaustive survey for Japanese volcanoes. *J. Geophys. Res. Atmos.* 118(15):8662–74

Mukhopadhyay S. 2012. Early differentiation and volatile accretion recorded in deep-mantle neon and xenon. *Nature* 486(7401):101–4

Muramatsu Y, Doi T, Tomaru H, Fehn U, Takeuchi R, Matsumoto R. 2007. Halogen concentrations in pore waters and sediments of the Nankai Trough, Japan: implications for the origin of gas hydrates. *Appl. Geochem.* 22(3):534–56

Muramatsu Y, Wedepohl KH. 1998. The distribution of iodine in the earth's crust. *Chem. Geol.* 147(3–4):201–16

Nestola F, Smyth JR. 2016. Diamonds and water in the deep Earth: a new scenario. *Int. Geol. Rev.* 58(3):263–76

Nichols ARL, Carroll MR, Höskuldsson A. 2002. Is the Iceland hot spot also wet? Evidence from the water contents of undegassed submarine and subglacial pillow basalts. *Earth Planet. Sci. Lett.* 202(1):77–87

Nielsen SG, Shimizu N, Lee CTA, Behn MD. 2014. Chalcophile behavior of thallium during MORB melting and implications for the sulfur content of the mantle. *Geochem. Geophys. Geosyst.* 15(12):4905–19

Ozima M, Podosek FA. 2002. *Noble Gas Geochemistry*. Cambridge, UK: Cambridge Univ. Press

Palot M, Cartigny P, Harris JW, Kaminsky FV, Stachel T. 2012. Evidence for deep mantle convection and primordial heterogeneity from nitrogen and carbon stable isotopes in diamond. *Earth Planet. Sci. Lett.* 357:179–93

Parai R, Mukhopadhyay S. 2012. How large is the subducted water flux? New constraints on mantle regassing rates. *Earth Planet. Sci. Lett.* 317:39–406

Parai R, Mukhopadhyay S. 2015. The evolution of MORB and plume mantle volatile budgets: constraints from fission Xe isotopes in Southwest Indian Ridge basalts. *Geochem. Geophys. Geosyst.* 16(3):719–35

Parai R, Mukhopadhyay S. 2018. Xenon isotopic constraints on the history of volatile recycling into the mantle. *Nature* 560(7717):223–27

Investigated the evolution of Xe and H_2O subduction rates through time, using Xe isotope systematics.

Parai R, Mukhopadhyay S, Tucker JM, Pető MK. 2019. The emerging portrait of an ancient, heterogeneous and continuously evolving mantle plume source. *Lithos* 346:105153

Parsons B, Sclater JG. 1977. An analysis of the variation of ocean floor bathymetry and heat flow with age. *J. Geophys. Res.* 82(5):803–27

Pearson DG, Brenker FE, Nestola F, McNeill J, Nasdala L, et al. 2014. Hydrous mantle transition zone indicated by ringwoodite included within diamond. *Nature* 507(7491):221–24

Plank T. 2014. The chemical composition of subducting sediments. In *Treatise on Geochemistry*, ed. HD Holland, pp. 607–29. Amsterdam: Elsevier

Plank T, Kelley KA, Zimmer MM, Hauri EH, Wallace PJ. 2013. Why do mafic arc magmas contain ~4 wt% water on average? *Earth Planet. Sci. Lett.* 364:168–79

Plank T, Langmuir CH. 1998. The chemical composition of subducting sediment and its consequences for the crust and mantle. *Chem. Geol.* 145(3–4):325–94

Provides an updated and comprehensive overview of C influx and outflux pathways.

Plank T, Manning CE. 2019. Subducting carbon. *Nature* 574(7778):343–52

Porcelli D, Ballentine CJ. 2002. Models for distribution of terrestrial noble gases and evolution of the atmosphere. *Rev. Mineral. Geochem.* 47(1):411–80

Pyle DM, Mather TA. 2009. Halogens in igneous processes and their fluxes to the atmosphere and oceans from volcanic activity: a review. *Chem. Geol.* 263(1–4):110–21

Ranero CR, Morgan JP, McIntosh K, Reichert C. 2003. Bending-related faulting and mantle serpentinization at the Middle America trench. *Nature* 425(6956):367–73

Ratschbacher BC, Paterson SR, Fischer TP. 2019. Spatial and depth-dependent variations in magma volume addition and addition rates to continental arcs: application to global CO_2 fluxes since 750 Ma. *Geochem. Geophys. Geosyst.* 20(6):2997–3018

Resing JA, Lupton JE, Feely RA, Lilley MD. 2004. CO_2 and ^3He in hydrothermal plumes: implications for mid-ocean ridge CO_2 flux. *Earth Planet. Sci. Lett.* 226(3–4):449–64

Richardson SH, Shirey SB, Harris JW, Carlson RW. 2001. Archean subduction recorded by Re–Os isotopes in eclogitic sulfide inclusions in Kimberley diamonds. *Earth Planet. Sci. Lett.* 191(3–4):257–66

Roberge M, Bureau H, Bolfan-Casanova N, Frost DJ, Raepsaet C, et al. 2015. Is the transition zone a deep reservoir for fluorine? *Earth Planet. Sci. Lett.* 429:25–32

Rubie DC, Jacobson SA, Morbidelli A, O'Brien DP, Young ED, et al. 2015. Accretion and differentiation of the terrestrial planets with implications for the compositions of early-formed Solar System bodies and accretion of water. *Icarus* 248:89–108

Ruscitto DM, Wallace PJ, Cooper LB, Plank T. 2012. Global variations in H_2O/Ce: 2. Relationships to arc magma geochemistry and volatile fluxes. *Geochem. Geophys. Geosyst.* 13(3):Q03025

Saal AE, Hauri EH, Langmuir CH, Perfit MR. 2002. Vapour undersaturation in primitive mid-ocean-ridge basalt and the volatile content of Earth's upper-mantle. *Nature* 419(6906):451–55

Saffer DM, Tobin HJ. 2011. Hydrogeology and mechanics of subduction zone forearcs: fluid flow and pore pressure. *Annu. Rev. Earth Planet. Sci.* 39:157–86

Salters VJ, Stracke A. 2004. Composition of the depleted mantle. *Geochem. Geophys. Geosyst.* 5(5):Q05B07

Sano Y, Williams SN. 1996. Fluxes of mantle and subducted carbon along convergent plate boundaries. *Geophys. Res. Lett.* 23(20):2749–52

Schaefer L, Lodders K, Fegley B. 2012. Vaporization of the Earth: application to exoplanet atmospheres. *Astrophys. J.* 755(1):41

Shaw AM, Hauri EH, Behn MD, Hilton DR, Macpherson CG, Sinton JM. 2012. Long-term preservation of slab signatures in the mantle inferred from hydrogen isotopes. *Nat. Geosci.* 5(3):224–28

Shinohara H. 2013. Composition of volcanic gases emitted during repeating Vulcanian eruption stage of Shinmoedake, Kirishima volcano, Japan. *Earth Planets Space* 65(6):667–75

Shirey SB, Richardson SH. 2011. Start of the Wilson cycle at 3 Ga shown by diamonds from subcontinental mantle. *Science* 333(6041):434–36

Simons K, Dixon J, Schilling JG, Kingsley R, Poreda R. 2002. Volatiles in basaltic glasses from the Easter-Salas y Gomez seamount chain and Easter microplate: implications for geochemical cycling of volatile elements. *Geochem. Geophys. Geosyst.* 3:1039

Smart KA, Tappe S, Stern RA, Webb SJ, Ashwal LD. 2016. Early Archaean tectonics and mantle redox recorded in Witwatersrand diamonds. *Nat. Geosci.* 9(3):255–59

Smithsonian Inst. 2013. Global volcanism program. *Smithsonian Institution*. **https://volcano.si.edu/gvp_votw.cfm**

Sobolev AV, Asafov EV, Gurenko AA, Arndt NT, Batanova VG, et al. 2019. Deep hydrous mantle reservoir provides evidence for crustal recycling before 3.3 billion years ago. *Nature* 571(7766):555–59

Staudacher T, Allègre CJ. 1988. Recycling of oceanic crust and sediments: the noble gas subduction barrier. *Earth Planet. Sci. Lett.* 89(2):173–83

Straub SM, Layne GD. 2003. The systematics of chlorine, fluorine, and water in Izu arc front volcanic rocks: implications for volatile recycling in subduction zones. *Geochim. Cosmochim. Acta* 67(21):4179–203

Stroncik NA, Haase KM. 2004. Chlorine in oceanic intraplate basalts: constraints on mantle sources and recycling processes. *Geology* 32(11):945–48

Thomson AR, Walter MJ, Kohn SC, Brooker RA. 2016. Slab melting as a barrier to deep carbon subduction. *Nature* 529(7584):76–79

Tollstrup D, Gill J, Kent A, Prinkey D, Williams R, et al. 2010. Across-arc geochemical trends in the Izu-Bonin arc: contributions from the subducting slab, revisited. *Geochem. Geophys. Geosyst.* 11(1):Q01X10

Trieloff M, Kunz J, Allègre CJ. 2002. Noble gas systematics of the Réunion mantle plume source and the origin of primordial noble gases in Earth's mantle. *Earth Planet. Sci. Lett.* 200(3–4):297–313

Tucker JM, Hauri EH, Pietruszka AJ, Garcia MO, Marske JP, Trusdell FA. 2019. A high carbon content of the Hawaiian mantle from olivine-hosted melt inclusions. *Geochim. Cosmochim. Acta* 254:156–72

Turner SJ, Langmuir CH. 2015. What processes control the chemical compositions of arc front stratovolcanoes? *Geochem. Geophys. Geosyst.* 16(6):1865–93

Ulmer P, Trommsdorff V. 1995. Serpentine stability to mantle depths and subduction-related magmatism. *Science* 268(5212):858–61

Unni CK, Schilling JG. 1978. Cl and Br degassing by volcanism along the Reykjanes Ridge and Iceland. *Nature* 272(5648):19–23

van Hunen J, Moyen JF. 2012. Archean subduction: fact or fiction? *Annu. Rev. Earth Planet. Sci.* 40:195–219

van Keken PE, Wada I, Abers GA, Hacker BR, Wang K. 2018. Mafic high-pressure rocks are preferentially exhumed from warm subduction settings. *Geochem. Geophys. Geosyst.* 19(9):2934–61

von Huene R, Ranero CR, Vannucchi P. 2004. Generic model of subduction erosion. *Geology* 32(10):913–16

Wallace PJ. 1998. Water and partial melting in mantle plumes: inferences from the dissolved H_2O concentrations of Hawaiian basaltic magmas. *Geophys. Res. Lett.* 25(19):3639–42

Wallace PJ. 2005. Volatiles in subduction zone magmas: concentrations and fluxes based on melt inclusion and volcanic gas data. *J. Volcanol. Geotherm. Res.* 140(1–3):217–40

Walter MJ, Bulanova GP, Armstrong LS, Keshav S, Blundy JD, et al. 2008. Primary carbonatite melt from deeply subducted oceanic crust. *Nature* 454(7204):622–25

Wang H, Weiss BP, Bai XN, Downey BG, Wang J, et al. 2017. Lifetime of the solar nebula constrained by meteorite paleomagnetism. *Science* 355(6325):623–27

Warren JK. 2010. Evaporites through time: tectonic, climatic and eustatic controls in marine and nonmarine deposits. *Earth-Sci. Rev.* 98(3–4):217–68

Watenphul A, Wunder B, Heinrich W. 2009. High-pressure ammonium-bearing silicates: implications for nitrogen and hydrogen storage in the Earth's mantle. *Am. Mineral.* 94(2–3):283–92

Werner C, Fischer TP, Aiuppa A, Edmonds M, Cardellini C, et al. 2019. Carbon dioxide emissions from subaerial volcanic regions. In *Deep Carbon: Past to Present*, ed. BN Orcutt, I Daniel, R Dasgupta, pp. 188–236. New York: Cambridge Univ. Press

White WM. 2010. Oceanic island basalts and mantle plumes: the geochemical perspective. *Annu. Rev. Earth Planet. Sci.* 38:133–60

Williams CD, Mukhopadhyay S. 2019. Capture of nebular gases during Earth's accretion is preserved in deep-mantle neon. *Nature* 565(7737):78–81

Wilson CR, Spiegelman M, van Keken PE, Hacker BR. 2014. Fluid flow in subduction zones: the role of solid rheology and compaction pressure. *Earth Planet. Sci. Lett.* 401:261–74

Workman RK, Hart SR. 2005. Major and trace element composition of the depleted MORB mantle (DMM). *Earth Planet. Sci. Lett.* 231(1–2):53–72

Workman RK, Hauri E, Hart SR, Wang J, Blusztajn J. 2006. Volatile and trace elements in basaltic glasses from Samoa: implications for water distribution in the mantle. *Earth Planet. Sci. Lett.* 241(3–4):932–51

Wu J, Desch SJ, Schaefer L, Elkins-Tanton LT, Pahlevan K, Buseck PR. 2018. Origin of Earth's water: chondritic inheritance plus nebular ingassing and storage of hydrogen in the core. *J. Geophys. Res. Planets* 123(10):2691–712

Yokochi R, Marty B. 2004. A determination of the neon isotopic composition of the deep mantle. *Earth Planet. Sci. Lett.* 225(1–2):77–88

Zhang C, Cai Y, Xu H, Dong Q, Liu J, Hao R. 2017. Mechanism of mineralization in the Changjiang uranium ore field, South China: evidence from fluid inclusions, hydrothermal alteration, and H–O isotopes. *Ore Geol. Rev.* 86:225–53

Zhang Z, Dorfman SM, Labidi J, Zhang S, Li M, et al. 2016. Primordial metallic melt in the deep mantle. *Geophys. Res. Lett.* 43(8):3693–99

Zindler A, Hart S. 1986. Chemical geodynamics. *Annu. Rev. Earth Planet. Sci.* 14:493–571

Annual Review
of Earth and
Planetary Sciences
Volume 49, 2021

Contents

Errata

An online log of corrections to *Annual Review of Earth and Planetary Sciences* articles may be found at http://www.annualreviews.org/errata/earth